Atmos. Chem. Phys., 10, 1133–1153, 2010
www.atmos-chem-phys.net/10/1133/2010/


Atmospheric Chemistry and Physics

# First multi-year occultation observations of $CO_2$ in the MLT by ACE satellite: observations and analysis using the extended CMAM

**S. R. Beagley**[1], **C. D. Boone**[2], **V. I. Fomichev**[1], **J. J. Jin**[1,*], **K. Semeniuk**[1], **J. C. McConnell**[1], **and P. F. Bernath**[2,3]

[1]Department of Earth and Space Science and Engineering, York University, Toronto, Ontario, Canada
[2]Department of Chemistry, University of Waterloo, Waterloo, Ontario, Canada
[3]Department of Chemistry, University of York, Heslington, York, UK
[*]currently at: Jet Propulsion Laboratory, California Institute of Technology, Pasadena, California, USA

Received: 6 March 2009 – Published in Atmos. Chem. Phys. Discuss.: 11 May 2009
Revised: 28 October 2009 – Accepted: 16 November 2009 – Published: 3 February 2010

**Abstract.** This paper presents the first global set of observations of $CO_2$ in the mesosphere and lower thermosphere (MLT) obtained by the ACE-FTS instrument on SCISAT-I, a small Canadian satellite launched in 2003. The observations use the solar occultation technique and document the fall-off in the mixing ratio of $CO_2$ in the MLT region. The beginning of the fall-off of the $CO_2$, or "knee" occurs at about 78 km and lies higher than in the CRISTA-1 measurements (∼70 km) but lower than in the SABER 1.06 (∼80 km) and much lower than in rocket measurements. We also present the measurements of CO obtained concurrently which provide important constraints for analysis. We have compared the ACE measurements with simulations of the $CO_2$ and CO distributions in the vertically extended version of the Canadian Middle Atmosphere Model (CMAM). Applying standard chemistry we find that we cannot get agreement between the model and ACE $CO_2$ observations although the CO observations are adequately reproduced. There appears to be about a 10 km offset compared to the observed ACE $CO_2$, with the model "knee" occurring too high. In analyzing the disagreement, we have investigated the variation of several parameters of interest (photolysis rates, formation rate for $CO_2$, and the impact of uncertainty in turbulent eddy diffusion) in order to explore parameter space for this problem. Our conclusions are that there must be a loss process for $CO_2$, about 2–4 times faster than photolysis that will sequester the carbon in some form other than CO and we have speculated on the role of meteoritic dust as a possible candidate. In addition, from this study we have highlighted a possible important role for unresolved vertical eddy diffusion in 3-D models in determining the distribution of candidate species in the mesosphere which requires further study.

*Correspondence to:* S. R. Beagley
(beagley@nimbus.yorku.ca)

## 1 Introduction

Carbon dioxide plays an important role in the energetics of the mesosphere and lower thermosphere (MLT) providing the major radiative cooling of the region; however its abundance in the MLT is still uncertain. It is generally considered to be well-mixed up to at least 70 km but starts to fall off at higher altitudes due to diffusive separation and photolysis. The first $CO_2$ measurements in the upper atmosphere were in-situ measurements obtained by rocket-borne mass spectrometers (Offermann and Grossmann, 1973; Philbrick et al., 1973; Trinks and Fricke, 1978; Offermann et al., 1981). Emission of the $CO_2$ $\nu_3$ band (asymmetric stretch mode) at 4.3 µm has also been obtained from rocket measurements (e.g., Nebel et al., 1994) and from satellite by the Stratospheric and Mesospheric Sounder (SAMS) (López-Puertas and Taylor, 1989) and Improved Stratospheric and Mesospheric Sounder (ISAMS) experiments (López-Puertas et al., 1998; Zaragoza et al., 2000) up to ∼120 km.

Global measurements of $CO_2$ have been obtained by the Cryogenic Infrared Spectrometers and Telescopes for the Atmosphere (CRISTA) experiment which was flown on two Space Shuttle missions in November 1994 and August 1997. CRISTA measured $CO_2$ 4.3 µm infrared emission and a non-local thermodynamic equilibrium (non-LTE) model was used to invert the radiances to $CO_2$ number densities in the

60–130 km range (Kaufmann et al., 2002). The CRISTA measurements showed that the $CO_2$ volume mixing ratio (VMR) deviated from a well mixed state between 70 km and 80 km. This initial deviation, which we call the "knee", is significantly lower in altitude than the results indicated by the rocket-borne mass spectrometer data mentioned above. The fact that $CO_2$ starts to deviate from the well mixed state lower in altitude, than the models predict, has been reported by various researchers in the past, and this is summarized in a review (López-Puertas et al., 2000).

More recently the Sounding of the Atmosphere using Broadband Emission Radiometery (SABER) experiment which measures 4.3 µm emission in the MLT region on the Thermosphere-Ionosphere-Mesosphere-Energetics and Dynamics (TIMED) satellite (e.g. Mertens et al., 2009b) has provided daytime $CO_2$ profiles using their version 1.06 (V1.06) retrieval method. However it should be mentioned that the $CO_2$ from SABER version 1.06 is very preliminary and not yet validated. For V1.06 retrievals their high latitude results are often compromised by the presence of $NO^+$ 4.3 µm emission due to electron precipitation in the auroral region. The SABER team have started to address this for V1.07 temperatures (cf. Mertens et al., 2009a; Remsberg et al., 2008) but $CO_2$ profiles necessary for V1.07 temperature retrievals are taken from model data.

The drawback of using emission measurements of the $\nu_3$ band at 4.3 µm is that this approach does not give direct information on the $CO_2$ abundance, but rather on the population of the vibrationally excited $\nu_3$ level. The mesosphere is a region where the breakdown of local thermodynamic equilibrium (LTE) conditions starts to occur meaning that in order to obtain the $CO_2$ abundance from emission measurements, non-LTE models must be used to interpret and invert the data. The population of the vibrationally excited $\nu_3$ level depends on the emission from this level, the absorption of near-infrared radiation emanating from the sun and from the lower atmosphere, and on collisional excitation and de-excitation by the background species, in particular by excited atomic oxygen, $O(^1D)$. There is also some evidence that highly vibrationally excited hydroxyl molecules affect the $CO_2$ asymmetric stretch mode (Kumer et al., 1978; Lopez-Puetas et al., 2004). In addition, as noted above (Mertens et al., 2009a; Remsberg et al., 2008), with broadband instruments there is the possibility of contamination from $NO^+$ 4.3 µm emission from aurora and the ionosphere. The complexity of the non-LTE retrieval is illustrated by the fact that Kaufmann et al. (2002) stated that along with the non-LTE model parameters, the $O(^1D)$ excitation mechanism constitutes the most important uncertainties of retrieved $CO_2$, whereas Edwards et al. (1996) gave rather small constraints for this excitation mechanism.

As mentioned above, emission instruments do not directly measure the ground state density of $CO_2$. However for solar occultation measurements, when transitions from the ground vibrational state is considered, the absorption only depends on the $CO_2$ ground state density, the kinetic temperature and the pressure and not on the vibrational excitation of the $CO_2$ molecule. Although some non-LTE effects in solar occultation measurement can occur through the vibrational partition function (Edwards et al., 1998), these effects are very small below about 100 km (errors related to the non-LTE vibrational partition function are discussed in Sect. 2.3). The drawback of solar occultation measurements, as compared to an emission experiment such as CRISTA-1, is the number of profiles obtained per day. For typical low earth orbit satellites there are about 30 profiles (sunrise and sunset) per day. Solar occultation measurements of $CO_2$ have been performed on board Spacelab 1 with the grille spectrometer (Girard et al., 1988) and on Spacelab 3 by the Atmospheric Trace Molecule Spectroscopy (ATMOS) instrument (Rinsland et al., 1992) and in the Atmospheric Laboratory for Applications and Science (ATLAS) 1, 2 and 3 missions (Kaye and Miller, 1996).

The accuracy of $CO_2$ measured by the grille spectrometer on Spacelab 1 was limited by the fact that they could not determine pressure and temperature profiles from their own measurements. They employed a modified version of the US Standard Atmosphere as inputs to their retrievals (Girard et al., 1988), and (potentially significant) errors in these assumed pressure and temperature profiles would lead to errors in the retrieved $CO_2$ VMR profile.

The ATMOS instrument had the benefit of determining pressure and temperature from its own measurements, just as the Fourier Transform Spectrometer (FTS) on the Canadian Atmospheric Chemistry Experiment (ACE) satellite SCISAT–1 (Bernath et al., 2005) does. However, the signal-to-noise ratio (SNR) for all but one of the occultations employed in the Spacelab 3 study (Rinsland et al., 1992) was about 74:1, much lower than that achieved by the ACE-FTS (about 350:1) in the spectral region of the strong $CO_2$ lines. The SNR for the other occultation used in the ATMOS study was close to 200:1. There were few occultations measured during the Spacelab 3 mission, yielding minimal opportunity for reducing random noise on the profiles through averaging.

## 2 ACE observations

The MLT $CO_2$ observations were obtained using the ACE-FTS instrument (Bernath et al., 2005). The ACE-FTS measures temperature and about thirty species involved in stratospheric ozone-related chemistry, tropospheric air quality as well as isotopologues of some of the molecules. ACE-FTS obtains solar occultations from 2.3 µm to 13.3 µm (750–4400 $cm^{-1}$) with a high spectral resolution (0.02 $cm^{-1}$). The vertical resolution is on average 3–4 km, but varies (from 2–6 km) with month, alternating from best to worst every other month and is best during both months analyzed in this paper, April and August.

### 2.1 Retrieval approach

The retrieval approach for temperature, pressure, and VMRs is described by Boone et al. (2005). Selected details of the retrieval approach will be reiterated here for clarity. The pressure/temperature ($P/T$) retrievals for the ACE-FTS employ the analysis of $CO_2$ microwindows, small (typically $\sim$0.4 $cm^{-1}$ wide) regions of the spectrum with minimal interference from other molecules. In order to minimize potential effects resulting from deviations from LTE, all microwindows above 65 km contain spectral lines from transitions originating in the ground vibrational state. Care is taken to avoid significant contributions in the microwindows from lines involving different lower state vibrations. Care is also taken to avoid interferences from different isotopologues of the molecule (e.g., $^{13}CO_2$) in the microwindows. $CO_2$ absorption is calculated using the spectroscopic parameters in the HITRAN 2004 linelist (Rothman et al., 2005).

At high altitudes (above $\sim$60 km), the tangent height separation between measurements is a known quantity, calculated from simple geometry and an accurate knowledge of the time difference between the measurements. Absolute time is known less accurately than the time difference between measurements, and so a registration approach is required to determine absolute altitude. Absolute tangent height is known to within about 150 m, while the spacing between tangent heights at high altitudes is accurate to better than 10 m, limited by the on-board clock's precision.

At high altitudes, $CO_2$ VMR and temperature are retrieved simultaneously. The relative transmittance of lines with different lower state rotational energies provides information on temperature, while the absolute values of the transmittance determine $CO_2$ VMR. However, the two parameters are highly correlated, due to the relationship of temperature to atmospheric density. In the absence of constraints, retrievals sometimes yield nonphysical oscillations in the $CO_2$ VMR profile, accompanied by compensating oscillations in the temperature profile. To avoid this, an empirical function was employed to describe the $CO_2$ VMR to introduce a smoothing constraint, thereby reducing the likelihood of nonphysical oscillations. The form of the empirical function adopted was:

$$CO_2\text{VMR}(z) = \frac{\text{VMR}_{\text{strat}} + a(z-z_o) + b(z-z_o)^2 + c(z-z_o)^3}{1 + d(z-z_o) + e(z-z_o)^2}, \quad (1)$$

where $a, b, c, d$, and $e$ are the empirical parameters determined through least-squares fitting, $z$ is altitude, $z_o$ is taken as the highest tangent height for which $CO_2$ VMR is assumed constant (around 60 km), and $\text{VMR}_{\text{strat}}$ is the assumed stratospheric value for $CO_2$. The value for $\text{VMR}_{\text{strat}}$ at a given time is calculated from the same equation used by the Halogen Occultation Experiment (HALOE) (Russell III et al., 1993). No provisions are made for variations with location or season. Above the highest analyzed measurement in the $P/T$ retrievals (around 125 km), the $CO_2$ VMR in Eq. (1) is taken as a constant as a function of altitude.

In ACE-FTS version 2.2 retrievals, $CO_2$ VMR in Eq. (1) was not constrained to approach the stratospheric value smoothly. This often led to a "step" in the $CO_2$ VMR profile near 60 km and gave rise to a systematic 3–5 K offset in retrieved temperature in the mesosphere (Sica et al., 2008). In the preliminary version 3.0 retrievals employed in the current study, this problem has been fixed.

During the $P/T$ retrieval, pressure is calculated from the retrieved temperature (and the known pointing geometry) through the equation for hydrostatic equilibrium:

$$\frac{dP}{dz} = -g(z)\rho(z) = -\frac{g(z)m_a(z)P(z)}{kT(z)}, \quad (2)$$

where $P$ is pressure, $z$ is altitude, $k$ is the Boltzmann constant, $T$ is temperature, $\rho$ is density, $g$ is the acceleration due to gravity, and $m_a$ is average molecular mass. The average molecular mass, $m_a$, is expected to be constant at lower altitudes, mostly from $N_2$ and $O_2$, but decreases because of the increased relative abundance of lower mass particles (mostly atomic oxygen). The variation with altitude for $m_a$ is taken from the MSIS atmosphere (Picone et al., 2002). The MSIS software was run for every occultation's location and time and using corresponding parameters of solar and magnetic activity. For convenience, the variation with altitude of $m_a$ is taken to be:

$$m_a(z) = \begin{cases} 28.94 \text{ atomic mass units} & z < 85\text{km} \\ a + bz + cz^2 + dz^3 + ez^4 + fz^5 & z \geq 85\text{km} \end{cases} \quad (3)$$

where the parameters $a$, $b$, $c$, $d$, $e$, and $f$ are determined by a least-squares fitting of the average mass as a function of altitude calculated from MSIS.

For calculating the pressure profile at high altitude, a single value for pressure is determined near 60 km, as described in Boone et al. (2005). Equation Eq. (2) is then integrated upward. Following this, atmospheric density is calculated from pressure and temperature via the ideal gas law using $m_a$.

The ACE-FTS instrumental line shape (ILS) suffers from a self-apodization of unknown source. A new form of the ILS was developed for version 3.0 of the ACE-FTS processing, where the empirical function used to account for the self-apodization was different than the form used for version 2.2 (Boone et al., 2005). The preliminary version 3.0 software employed in the current study featured this new ILS.

The maximum optical path difference for the ACE-FTS instrument is 25 cm. To calculate the ILS for the ACE-FTS, we first generate the nominal modulation function for the instrument, a rectangular function that is 1 for optical path differences between $\pm$25 cm and 0 for larger path differences. This rectangular function is multiplied by a *sinc* function to account for rays traveling off-axis due to the finite field of view (FOV) (Davis et al., 2001). In addition, we multiply

by the following empirical function to account for the self-apodization effects:

$$\exp(1)\exp\left(-\exp\left(\frac{ax^{10}}{1+bx^{10}}\right)\right)\left(1-c\frac{|x|}{\mathrm{MOPD}}\right), \quad (4)$$

where $x$ is optical path difference and MOPD is the maximum optical path difference. The variation with wavenumber for the self-apodization effects was accounted for by using an effective value for the instrument's FOV. The ILS is then calculated by taking the Fourier transform of the modulation function.

The empirical parameters $a, b$, and $c$ in Eq. (4) and the value for the effective FOV were determined by fitting lines at high altitude in the ACE-FTS spectrum, taking the average of the results derived from ∼100 different occultations. The two detector regions for the ACE-FTS were treated separately. For the Mercury Cadmium Telluride (MCT) detector region, covering the spectral range 750–1850 $cm^{-1}$, the values determined for the empirical parameters were $a = 4.403 \times 10^{-16}$, $b = -9.9165 \times 10^{-15}$, $c = 0.03853$, and effective FOV=7.591 mrad (as compared to the nominal value of 6.25 mrad). For the Indium Antimonide (InSb) detector region, 1850–4400 $cm^{-1}$, values determined for the empirical parameters were $a = 2.762 \times 10^{-16}$, $b = -1.009 \times 10^{-14}$, $c = 0.0956$, and effective FOV=7.865 mrad. Fitting residuals using this new ILS are typically several percent smaller than those obtained with the version 2.2 ILS.

### 2.2 Retrieval results

Employing software developed for the processing version 3.0 of the ACE-FTS, $P/T$ retrievals were performed for all occultations from February 2004 through August 2007. $CO_2$ VMR is a byproduct of $P/T$ retrievals, although the retrieved profile at high altitudes ($z > 60$ km) is smoothed through the use of the empirical function Eq. (1) during the retrieval.

Following the $P/T$ retrieval, "straight" retrievals for $CO_2$ (retrievals for $CO_2$ VMR with pressure, temperature, and density fixed to the results of the $P/T$ retrievals) were performed over the altitude range 50–120 km (∼1.0 to $2\times10^{-5}$ hPa) for the same set of occultations. In this case Eq. (1) was not used. The microwindows used in the straight retrievals are listed in Table 1. Transmittances in these microwindows range from roughly 2 to 50%. These same microwindows are employed in the $P/T$ retrievals in the given altitude region, although the $P/T$ retrievals extend lower than 50 km and there are additional microwindows in the $P/T$ retrievals that only contribute below 50 km.

The results of these straight $CO_2$ retrievals were obviously not independent from the $CO_2$ VMR profiles derived during the $P/T$ retrievals. One expects the same basic results from both retrievals, with more noise in the profiles from the straight retrievals due to the lack of smoothing. Differences between the two sets of results (averages over several occultations) would actually be of concern, suggestive of problems in the retrieval approach.

It is important to note that the results and conclusions of the present paper would be no different if we had used the data directly from the $P/T$ retrieval. The two datasets are equivalent, although the residuals from the straight retrievals are smaller than those from the $P/T$ retrievals, thanks to the removal of the smoothing constraint employed in the $P/T$ retrievals. Because the fitting residuals are smaller, the straight retrievals are technically more representative of the measurements.

All occultations from February 2004 through August 2007, and thus $CO_2$ VMR retrieved over the altitude range 50 to 120 km are used for our analysis. The ACE-FTS observations combining both sunrise and sunset occultations are shown in Fig. 1 and are averages of the period 21 February 2004 to 30 August 2007. The coverage is not uniform and reflects that the SCISAT-1 orbit was optimized to investigate the Arctic stratosphere in winter while obtaining reasonable coverage at lower latitudes. The data indicate a general fall-off of the $CO_2$ VMR with height in the upper mesosphere and lower thermosphere as may be expected from the loss processes (see below). The meridional $CO_2$ distribution for the solstice months appears to be consistent with the large-scale circulation exhibited by the extended Canadian Middle Atmosphere Model (CMAM). As reported by McLandress et al. (2006), the meridional wind in the CMAM is characterized by summer-to-winter flow in the mesosphere and winter-to-summer flow in the lower thermosphere between 100 and 120 km. The former is a feature of the thermally indirect circulation driven primarily by non-orographic gravity wave drag (GWD), whereas the meridional wind reversal in the lower thermosphere is a direct result of the resolved wave drag. This circulation pattern suggests that in the MLT subpolar summer region there should be upwelling in the lower and middle mesosphere and downwelling in the upper mesosphere. In agreement with this pattern, the January $CO_2$ data for the austral subpolar region appear to indicate the upwelling cell up to about 85 km ($\sim 5 \times 10^{-3}$ hPa) and downwelling cell in the region above, where the descending air brings down low $CO_2$ mixing ratios. This is also hinted at in the June/July data for boreal regions.

When examining Fig. 1, it should be noted that specific features in the $CO_2$ and CO datasets may not be accurately compared between the ACE and CMAM results at high latitudes, since the ACE experiment is subject to a sampling bias which can produce artifacts. This issue will be discussed later in the paper.

### 2.3 Error estimates

There are several contributions to the uncertainties for high-altitude $CO_2$ VMR retrievals from the ACE-FTS. Things are especially complicated by the fact that pressure and temperature are determined simultaneously with $CO_2$.

**Table 1.** ACE Microwindows and transistions.

| Center ($cm^{-1}$) | Width ($cm^{-1}$) | Lower limit (km) | Upper limit (km) | $E''$ ($cm^{-1}$) | Center ($cm^{-1}$) | Width ($cm^{-1}$) | Lower limit (km) | Upper limit (km) | $E''$ ($cm^{-1}$) |
|---|---|---|---|---|---|---|---|---|---|
| 1899.17 | 0.3 | 50 | 58 | 772.1 | 2361.45 | 0.3 | 90 | 120 | 106.1 |
| 1902.05 | 0.3 | 50 | 60 | 639.6 | 2364.1 | 0.3 | 90 | 120 | 163.9 |
| 1906.48 | 0.3 | 50 | 65 | 464.2 | 2366.63 | 0.3 | 90 | 120 | 234.1 |
| 1911.02 | 0.35 | 50 | 68 | 316.8 | 2367.88 | 0.3 | 90 | 120 | 273.9 |
| 1912.52 | 0.35 | 50 | 68 | 273.9 | 2369.1 | 0.3 | 90 | 120 | 316.8 |
| 1914.12 | 0.3 | 50 | 70 | 234.1 | 2370.27 | 0.35 | 90 | 120 | 362.8 |
| 1915.48 | 0.3 | 50 | 70 | 197.4 | 2371.43 | 0.3 | 90 | 120 | 411.9 |
| 1917.06 | 0.35 | 50 | 70 | 163.9 | 2372.56 | 0.3 | 90 | 120 | 464.2 |
| 1920.11 | 0.35 | 50 | 70 | 106.1 | 2373.67 | 0.35 | 90 | 120 | 519.5 |
| 1924.71 | 0.35 | 50 | 65 | 42.9 | 2374.23 | 0.28 | 50 | 65 | 2292.6 |
| 1933.98 | 0.24 | 50 | 60 | 411.9 | 2374.75 | 0.4 | 90 | 120 | 578.0 |
| 2044.5 | 0.3 | 50 | 70 | 704.3 | 2375.4 | 0.28 | 50 | 60 | 2444.3 |
| 2045.97 | 0.3 | 53 | 73 | 639.6 | 2375.8 | 0.35 | 90 | 120 | 639.6 |
| 2047.53 | 0.4 | 55 | 73 | 578.0 | 2376.84 | 0.35 | 90 | 120 | 704.3 |
| 2049.05 | 0.4 | 53 | 75 | 519.5 | 2377.85 | 0.35 | 90 | 120 | 772.1 |
| 2050.55 | 0.4 | 55 | 78 | 464.2 | 2378.83 | 0.35 | 75 | 120 | 843.0 |
| 2052.1 | 0.3 | 50 | 79 | 411.9 | 2379.78 | 0.35 | 90 | 120 | 917.1 |
| 2053.66 | 0.3 | 55 | 80 | 362.8 | 2380.72 | 0.35 | 85 | 115 | 994.2 |
| 2055.11 | 0.35 | 60 | 80 | 316.8 | 2381.62 | 0.35 | 85 | 115 | 1074.4 |
| 2056.72 | 0.3 | 55 | 85 | 273.9 | 2382.48 | 0.4 | 82 | 115 | 1157.8 |
| 2058.24 | 0.4 | 55 | 85 | 234.1 | 2383.36 | 0.35 | 82 | 115 | 1244.2 |
| 2061.33 | 0.35 | 60 | 85 | 163.9 | 2385.02 | 0.4 | 75 | 95 | 1426.4 |
| 2062.87 | 0.35 | 60 | 85 | 133.4 | 2385.79 | 0.35 | 73 | 90 | 1522.2 |
| 2066.03 | 0.35 | 60 | 85 | 81.9 | 2386.51 | 0.35 | 70 | 86 | 1621.0 |
| 2067.52 | 0.35 | 60 | 83 | 60.9 | 2387.26 | 0.35 | 65 | 83 | 1722.9 |
| 2070.65 | 0.4 | 62 | 80 | 28.1 | 2387.96 | 0.35 | 60 | 80 | 1828.0 |
| 2072.23 | 0.3 | 57 | 80 | 16.4 | 2388.64 | 0.35 | 55 | 77 | 1936.1 |
| 2293.9 | 0.35 | 78 | 94 | 1333.8 | 2389.29 | 0.35 | 50 | 71 | 2047.3 |
| 2300.4 | 0.3 | 90 | 115 | 1074.4 | 2389.92 | 0.3 | 50 | 68 | 2161.6 |
| 2306.85 | 0.3 | 95 | 120 | 843.0 | 2390.52 | 0.35 | 50 | 65 | 2279.0 |
| 2313.1 | 0.35 | 95 | 120 | 639.6 | 2391.13 | 0.3 | 50 | 62 | 2399.5 |
| 2319.14 | 0.26 | 90 | 120 | 464.2 | 2391.7 | 0.3 | 50 | 60 | 2523.0 |
| 2332.37 | 0.3 | 95 | 120 | 163.9 | 2392.1 | 0.3 | 50 | 55 | 2649.7 |
| 2354.37 | 0.26 | 90 | 120 | 16.4 | | | | | |

$E''$ – the energy of the lower state involved in the transition

Estimates for the errors from various sources are presented in Table 2 in terms of percentage. Error estimates were performed using a set of 20 occultations near latitude 30° N in April and including occultations from 2005–2007. The fitting errors in Table 2 (column "Random Errors") are the average errors for the 20 occultations from the least squares process (the square root of the diagonal elements in the covariance matrix) in the straight $CO_2$ VMR retrievals. All other error sources described here are systematic and their combined effect is given in the column "Total Systematic Error". To estimate each of the systematic errors, $P/T$ retrievals were performed in the set of 20 occultations with the indicated parameters changed as described below, and the uncertainties were taken as the average difference in $CO_2$ VMR compared to the original set of $P/T$ retrievals.

The column labeled "External domain $CO_2$" shows the combined errors arising from assumptions for the $CO_2$ VMR outside of the retrieval domain, below 60 km and above 125 km. $CO_2$ VMR below about 60 km is fixed in the retrieval. Errors in this quantity will lead to errors in the retrieved profile. The errors from this source were estimated by increasing the value of stratospheric $CO_2$ by 2%. The 2% is based on ATMOS data for a lower atmospheric $CO_2$ VMR uncertainty of 5.6 ppmv (López-Puertas, personal communication). The $CO_2$ VMR profile above 125 km, the highest analyzed measurement, is taken as a constant in altitude. The errors from this source were estimated by using a shaped profile, with $CO_2$ decreasing with altitude from ∼320 ppmv at 125 km to ∼240 and ∼140 ppmv at 135 and 150 km, respectively (data based on measurements

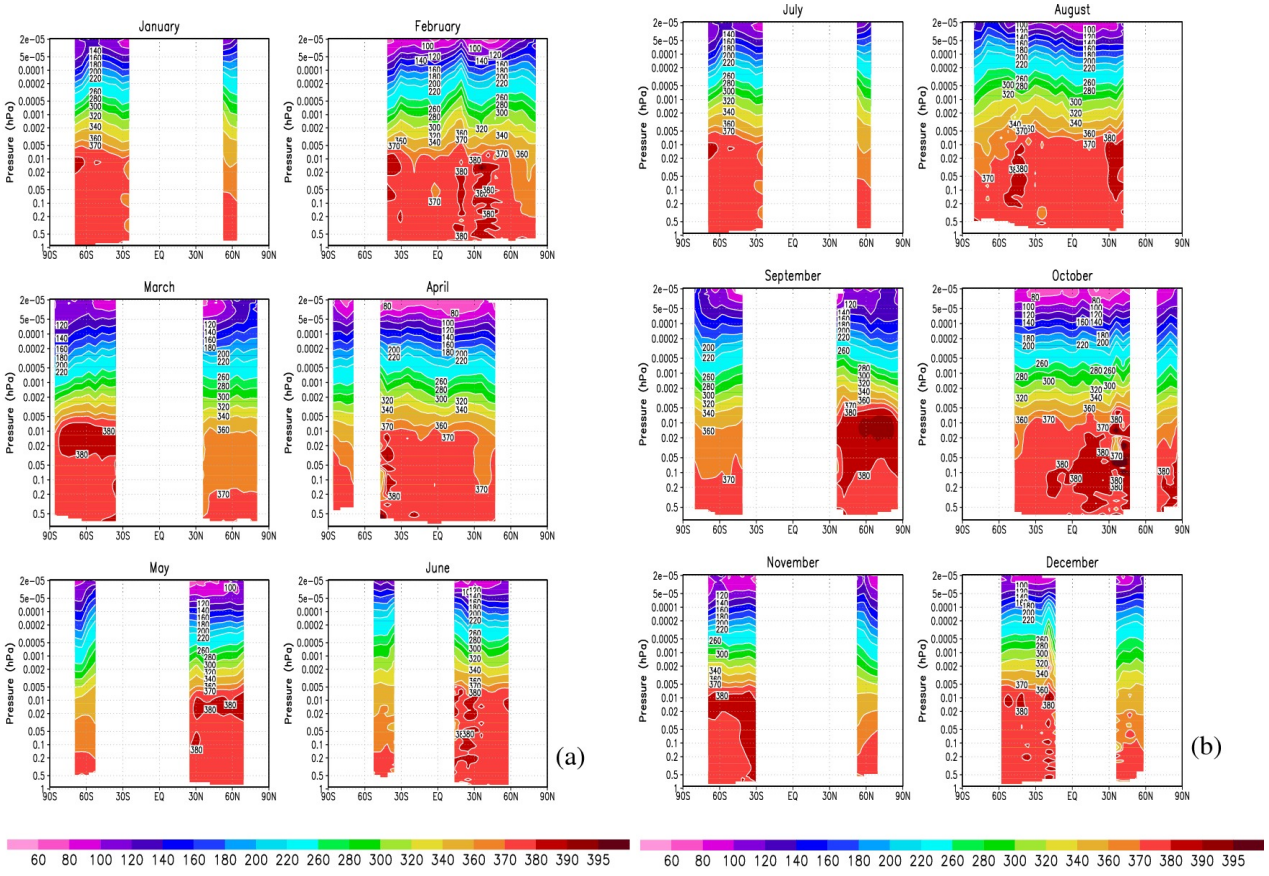


**Fig. 1.** Zonally and monthly averaged ACE $CO_2$ data (sunrise and sunset) for the period 21 February 2004 to 30 August 2007 versus latitude and pressure. The units are ppmv for the $CO_2$ mixing ratio, **(a)** January–June and **(b)** July–December.

and models; López-Puertas, personal communication). In the column labeled "External Domain $CO_2$", the errors below ∼80 km are mainly attributed to the uncertainties in the stratospheric $CO_2$ that is of the order 2%, whereas above 90 km the errors are attributed to the assumption of constant $CO_2$ VMR above 125 km.

In the HITRAN 2004 linelist, the uncertainties listed for the intensities of all the $CO_2$ lines employed in this study are 2–5%. To estimate errors from this source, the intensities for all $CO_2$ lines were decreased by 4%. The estimated errors are shown in the column labeled "Intensities" in Table 2. Uncertainties in the $CO_2$ spectroscopic constants from HITRAN 2004 are not included in the error estimate.

For the column labeled "ILS" in Table 2, the empirical parameters $a, b$, and $c$ in Eq. (4) were all decreased by 5%, while the effective FOV was increased by 2%, (based on standard deviation evaluations of the 100 occultation set). The scatter in values obtained for these parameters in the original analysis (using ∼100 occultations) were at least a factor of two smaller. However, the empirical function is not necessarily the best possible representation of the ILS, especially since its form is not based on any physical process. Therefore, errors on the ILS parameters were inflated in an ad hoc effort to account for additional uncertainties from deficiencies in the chosen form of the empirical function.

The analysis described here uses only $CO_2$ lines in the ground vibrational state, but deviations from LTE will still have some effect through changes in the vibrational partition function (Edwards et al., 1998). The column labeled "Non-LTE" in Table 2 adjusts the partition function using the results shown in Fig. 2 of Edwards et al. (1998).

The convergence criterion used in the ACE-FTS processing software is that chi-squared should change by less than one part in $10^4$ between steps in the least-squares fitting process. The column labeled "Convergence" in Table 2 uses a convergence criterion of one part in $10^6$.

The column "Other Systematic Errors" in Table 2 includes the combined errors from different sources described below. An individual error for any of these sources does not exceed 2%.

Knowledge of the average molecular mass, $m_a$ in Eq. (2), as a function of altitude is required to perform $P/T$ retrievals. Errors in this quantity will lead to errors in retrieved $CO_2$ VMR at high altitude. The variation with altitude for this

parameter is taken from the outputs of the MSIS software. In order to generate the error estimate, the average mass in the $P/T$ retrievals was fixed to 28.93 atomic mass units at all altitudes. This is likely an overestimate for this error source.

A linear dependence for the variation of acceleration due to gravity with altitude, $g(z)$ in Eq. (2), is employed in calculating pressure from hydrostatic equilibrium. Discrepancies between $g(z)$ calculated from this approximate form and the true acceleration due to gravity will lead to errors in retrieved $CO_2$ VMR. To estimate this errors, $P/T$ retrievals were performed with use of a more accurate expression for $g(z)$ dependence.

For the reporting of results the latitude of a given occultation is taken as the latitude corresponding to the ACE-FTS measurement nearest altitude 30 km. However, the latitude of the tangent point for an ACE-FTS measurement varies with altitude. The latitude of the occultation is used to assign effective gravity taken from the World Geodetic System (WGS) 84 model (European Organization for the safety of Air Navigation et al., 1998), which will modify the calculations using hydrostatic equilibrium. For the set of 20 occultations used to evaluate uncertainties, the latitude of the tangent point for measurements near 120 km was 2.5 to 2.8 degrees higher than the "30 km latitude" assigned to the occultation. An estimate of the error associated with a varying occultation latitude was generated by adding 3 degrees to the latitudes of the occultations in the $P/T$ retrievals.

Although the temperature profiles generated with the new version of the software should represent an improvement over the results from version 2.2, no formal validation of the new results has been carried out. Therefore for this paper we have used the estimates for the uncertainties due to errors in temperature based on the results of the validation of the version 2.2 results. Thus at the end of the high-altitude portion of the $P/T$ retrieval (where $CO_2$ VMR is determined), 2 K was added to the temperatures below 60 km and 5 K was added to temperatures above 60 km, and then $CO_2$ VMR was re-determined, using a least squares fitting only for the five parameters in the empirical function used for the VMR profile. These temperature error estimates are those reported in the ACE temperature validation paper (Sica et al., 2008). Note that density was changed in inverse proportion to the change in temperature, in order to retain internal consistency. Above the mesopause, temperature changes rapidly with altitude, and a temperature uncertainty of 5 K might be an underestimate. If this is true, the uncertainty at higher altitudes from this source have been also underestimated.

The total estimated errors on $CO_2$ in VMR, that is a combination of random and systematic errors, are shown as error bars in Figs. 2 and 4. The total errors are generally less then 10% below 100 km.

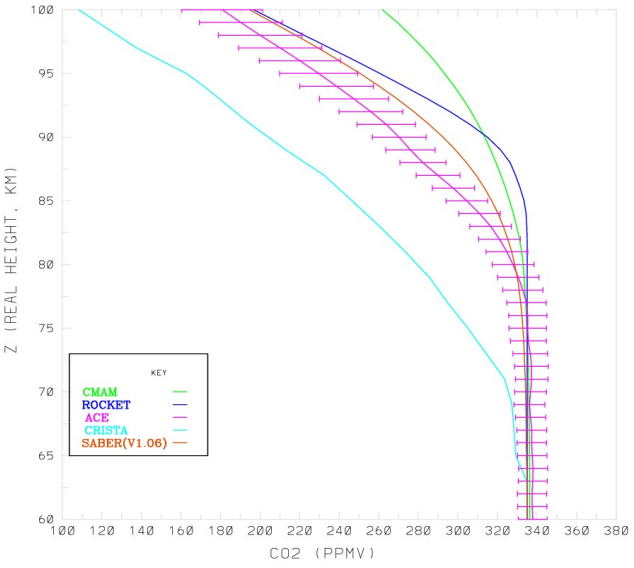


**Fig. 2.** A comparison of mean rocket measurements (compilation by Fomichev et al., 1998), global mean CRISTA observations (Kaufmann et al., 2002), daytime V1.06 SABER observations (see text for details), global mean ACE measurements and global mean CMAM $CO_2$. Error bars indicate the $CO_2$ uncertainties in ACE measurements.

## 3 Model

For the analysis we have used the extended CMAM (Beagley et al., 2000; Fomichev et al., 2002; McLandress et al., 2006) with a top at $2\times10^{-7}$ hPa (geopotential height ~220 km but dependent on the solar cycle) that was enhanced by inclusion of neutral and ion chemistry. The first version of the model included the non-LTE parameterization for the 15 µm $CO_2$ band, solar heating due to absorption by $O_2$ in the Schumann-Runge bands (SRB) and continuum (SRC), and by $O_2$, $N_2$ and O in the extreme ultraviolet spectral region, parameterized chemical heating, molecular diffusion and viscosity and ion drag. The current version of the extended CMAM also includes comprehensive stratospheric chemistry (e.g., de Grandpré et al., 2000) with radiatively interactive $O_3$ and $H_2O$, a simplified ion chemistry scheme (Beagley et al., 2007) over a vertically limited domain, and non-LTE treatment of the near-infrared $CO_2$ heating (Ogibalov and Fomichev, 2003). The Hines (1997a, b) non-orographic GWD scheme used in the model includes the impact of turbulence generated by the wave breaking on the momentum budget, thermal diffusion and allows for diffusive transport of minor species; this eddy diffusion we call $K_{zz}$ (GWD). The model also has a $K_{zz}$ resulting from wind shear and a background value of $K_{zz}$ for numerical control, the sum of both is generally less than $0.2\,m^2\,s^{-1}$. Above ~90 km vertical diffusive mixing is dominated by molecular diffusion. In addition to the parameterized diffusion, tracers in the model experience mixing from resolved dynamical processes

**Table 2.** ACE $CO_2$ measurement error estimates (in percentage).

| Altitude (km) | External Domain $CO_2$ | Intensities | ILS | Non-LTE | Convergence | Other Systematic Errors | Total Systematic Errors | Random Errors |
|---|---|---|---|---|---|---|---|---|
| 50.50 | 1.96 | 0 | 0 | 0 | 0 | 0 | 1.96 | 2.34 |
| 52.50 | 1.96 | 0 | 0 | 0 | 0 | 0 | 1.96 | 2.30 |
| 54.50 | 1.96 | 0 | 0 | 0 | 0 | 0 | 1.96 | 2.29 |
| 56.50 | 1.96 | 0 | 0 | 0 | 0 | 0 | 1.96 | 2.35 |
| 58.50 | 1.96 | 0.02 | 0.01 | 0.03 | 0 | 0.02 | 1.96 | 2.35 |
| 60.50 | 1.94 | 0.03 | 0 | 0.02 | −0.01 | 0.02 | 1.94 | 2.52 |
| 62.50 | 1.94 | 0.06 | 0 | 0.03 | 0 | 0.04 | 1.94 | 2.55 |
| 64.50 | 1.94 | 0.13 | −0.02 | 0.02 | 0.06 | 0.07 | 1.94 | 2.82 |
| 66.50 | 1.95 | 0.22 | −0.03 | −0.01 | 0.14 | 0.12 | 1.97 | 2.84 |
| 68.50 | 1.97 | 0.34 | −0.04 | −0.05 | 0.24 | 0.19 | 2.02 | 3.14 |
| 70.50 | 2.01 | 0.49 | −0.05 | −0.10 | 0.37 | 0.28 | 2.12 | 3.27 |
| 72.50 | 2.06 | 0.66 | −0.04 | −0.17 | 0.52 | 0.38 | 2.26 | 3.72 |
| 74.50 | 2.11 | 0.84 | −0.02 | −0.25 | 0.68 | 0.51 | 2.44 | 3.96 |
| 76.50 | 2.14 | 1.03 | 0.03 | −0.34 | 0.84 | 0.64 | 2.62 | 4.35 |
| 78.50 | 2.11 | 1.22 | 0.12 | −0.45 | 0.98 | 0.79 | 2.78 | 4.52 |
| 80.50 | 2.02 | 1.37 | 0.25 | −0.56 | 1.10 | 0.95 | 2.90 | 4.53 |
| 82.50 | 1.84 | 1.48 | 0.44 | −0.68 | 1.16 | 1.11 | 2.97 | 4.53 |
| 84.50 | 1.66 | 1.52 | 0.69 | −0.79 | 1.15 | 1.27 | 3.02 | 4.72 |
| 86.5 | 1.70 | 1.47 | 1.01 | −0.90 | 1.07 | 1.44 | 3.18 | 4.85 |
| 88.50 | 2.21 | 1.34 | 1.40 | −0.99 | 0.89 | 1.60 | 3.60 | 4.29 |
| 90.50 | 3.17 | 1.13 | 1.83 | −1.08 | 0.63 | 1.74 | 4.39 | 4.38 |
| 92.50 | 4.39 | 0.84 | 2.29 | −1.14 | 0.29 | 1.86 | 5.48 | 3.65 |
| 94.50 | 5.67 | 0.49 | 2.75 | −1.18 | −0.12 | 1.94 | 6.72 | 3.56 |
| 96.50 | 6.85 | 0.10 | 3.17 | −1.21 | −0.58 | 1.98 | 7.92 | 3.01 |
| 98.50 | 7.76 | −0.31 | 3.52 | −1.23 | −1.06 | 2.00 | 8.90 | 3.10 |
| 100.50 | 8.23 | −0.73 | 3.76 | −1.27 | −1.54 | 2.06 | 9.52 | 2.57 |
| 102.50 | 8.16 | −1.14 | 3.85 | −1.38 | −1.97 | 2.21 | 9.66 | 2.56 |
| 104.50 | 7.44 | −1.51 | 3.78 | −1.59 | −2.32 | 2.42 | 9.26 | 2.19 |
| 106.50 | 6.09 | −1.81 | 3.53 | −1.98 | −2.54 | 2.62 | 8.37 | 2.09 |
| 108.50 | 4.23 | −2.00 | 3.12 | −2.62 | −2.57 | 2.70 | 7.24 | 1.80 |
| 110.50 | 2.23 | −2.03 | 2.57 | −3.58 | −2.39 | 2.60 | 6.40 | 1.91 |
| 112.50 | 0.95 | −1.84 | 1.96 | −4.95 | −2.01 | 2.37 | 6.51 | 2.07 |
| 114.50 | 1.01 | −1.42 | 1.37 | −6.83 | −1.50 | 2.41 | 7.72 | 2.55 |
| 116.50 | 3.19 | −0.74 | 0.94 | −9.29 | −0.96 | 3.44 | 10.52 | 3.03 |
| 118.50 | 8.64 | 0.15 | 0.79 | −12.38 | −0.52 | 5.59 | 16.13 | 3.28 |

**Table 3.** Scenarios assumed.

| Scenario | Details |
|---|---|
| A (control) | $K_{zz}$ (GWD) included, standard rate constants and $J$ values |
| B | $J(CO_2)$ increased by 5, otherwise A |
| C | $K_{zz}$ (GWD) = 0, otherwise A |
| D | B + C |
| E | CO+OH reaction rate reduced by factor of 5, otherwise A |
| F | Molecular diffusion for $CO_2$ set to zero, otherwise A |

such as planetary waves, gravity waves and tides. This resolved diffusion is expected to be realistic. The dynamical code of the extended CMAM has been modified from the earlier version (Beagley et al., 2000; Fomichev et al., 2002; McLandress et al., 2006) to allow for a 7.5 min time step without the previously used height dependent time filter and enhanced horizontal diffusion in the thermosphere being required. The model configuration described above represents the standard conditions and we will explore modifications of the standard conditions below. In the text below this standard or control run is called scenario A and is listed in Table 3.

The chemistry of $CO_2$ in the model is straightforward. It consists of photolysis of $CO_2$ from wavelengths between 100–220 nm and $CO_2$ is reformed by reaction with OH, viz. CO+OH $\rightarrow$ H+$CO_2$. Between ∼65 km and 95 km the main destruction of $CO_2$ is photolysis by Lyman-$\alpha$ with loss in the SRB being important below 65 km and in the SRC being important above 95 km (e.g., Brasseur and Solomon, 2005). Although there is some uncertainty in the $CO_2$ cross

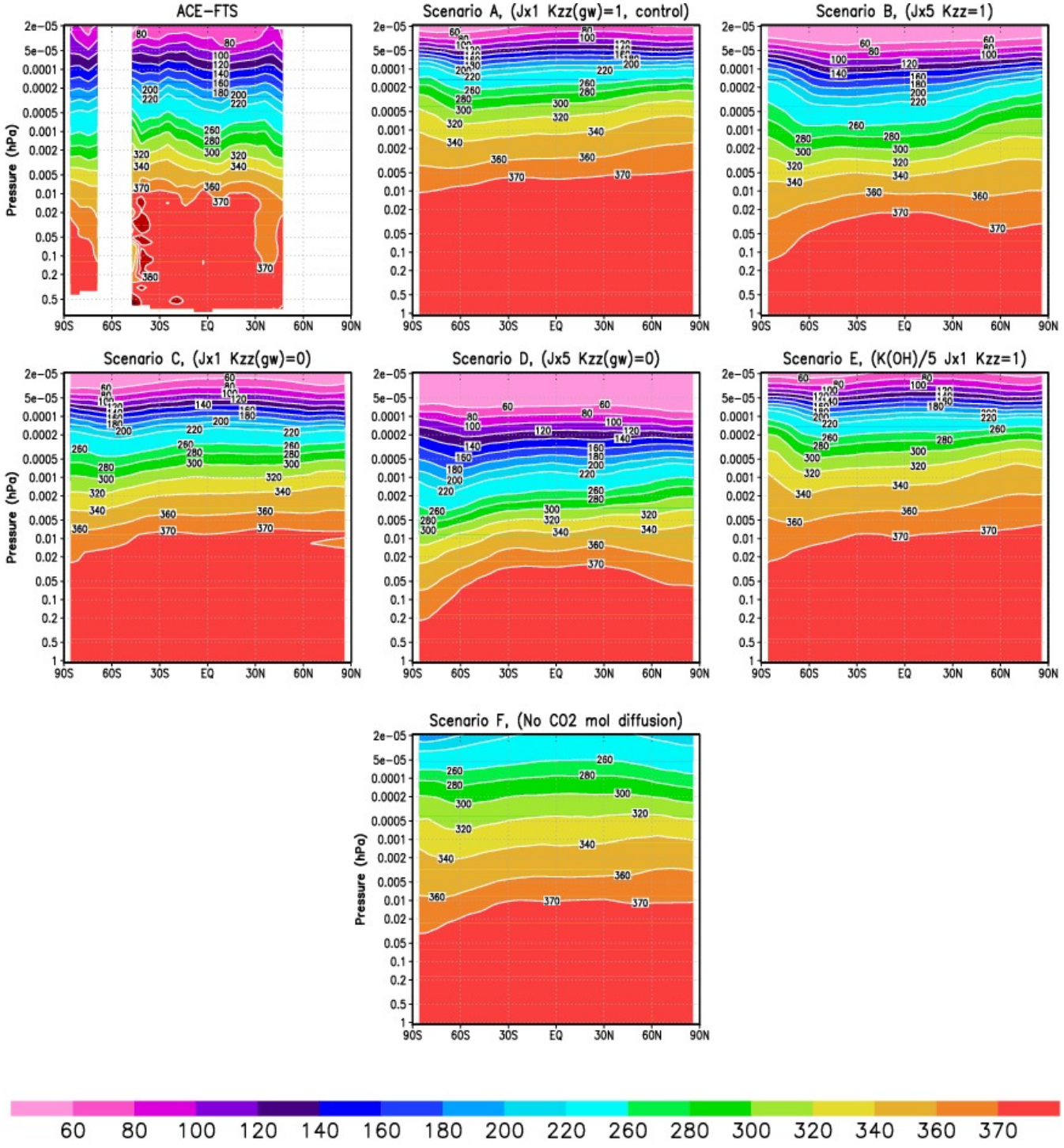


**Fig. 3.** Zonally and monthly averaged latitude-pressure plots of $CO_2$ volume mixing ratios (ppmv) for April for the different scenarios shown in Table 3 used for the CMAM and the ACE data (details same as Fig. 1).

section at the longer wavelengths which would affect photolysis below 65 km, the photolysis in the main region of interest, Lyman-$\alpha$, is generally well characterized. In any case we discuss the impact of the uncertainties below. As a result of $CO_2$ photolysis, CO is formed at all wavelengths with unit efficiency. Below about 45 km CO is produced by oxidation of $CH_4$.

In the analysis we shall make use of the intimate connection between CO and $CO_2$ in order to provide constraints on the possibilities for agreement between measurements and model. One other point to note is that the model simulations utilized a surface boundary condition of 335 ppmv while the background $CO_2$ for the ACE measurements is about 375 ppmv. In order to compare the vertical structures, we have scaled, in the plots, the model CO and $CO_2$ values by this ratio to match the observations.

## 4 Results

In the following we compare the ACE measurements with the CMAM results. But first we compare the ACE measurements with other experimental data including both optical and in-situ measurements from CRISTA-1, SABER and rockets. Figure 2 shows a mean $CO_2$ profile based on a compilation of rocket measurements (Fomichev et al., 1998), a global mean of the CRISTA-1 measurements (Kaufmann et al., 2002), a daytime global mean (V1.06) of the SABER measurements and a global mean of the ACE measurements. The rationale for choosing the CRISTA and SABER in the comparison is that like the ACE data both these datasets provide nearly global coverage. The rocket $CO_2$ profile shown here is that used in the non-interactive CMAM simulations. Even though there are latitudinal variations in the $CO_2$ distribution (Fig. 1) it is clear that these differences are much less than the differences between the various measurements and the model. The CMAM global results indicate a gradual fall-off above 80–85 km and, in general, the rate of fall-off is slower than for all the measurements except for the average rocket profile. Although above 90 km the rocket measurements also fall off more rapidly than the model results. The various observations suggest an uncertainty in the location of the "knee". The CRISTA-1 measurements are the lowest with the "knee" commencing at ∼72 km, well below the ACE "knee" of about 78 km. Note however that the CRISTA-1 $CO_2$ VMR deviates significantly from its lower atmospheric value (with respect to the accuracy of the data) only above 80 km (Kaufmann, personal communication). Above ∼72 km the slope of the average CRISTA-1 and ACE results are similar. For the SABER results the "knee" occurs at ∼80 km, comparable to ACE measurements, but the SABER curve lies ∼20 ppmv higher than ACE above the "knee". For the rocket measurements the "knee" lies highest at ∼87 km. Clearly there is a discrepancy between the different experiments with ACE and daytime SABER (V1.06) being the closest. The various observations suggest an uncertainty in the location of the "knee". As we noted above the derivation of $CO_2$ profiles from emissions measurements requires a complex non-LTE model while rocket measurements could be compromised by sampling problems in the vicinity of the rocket skin. ACE measures the ground state of $CO_2$ and, hence, fewer physical assumptions are required to obtain the $CO_2$ abundance. The method is straightforward and the physics involved simpler.

Figure 3 shows a comparison between the ACE-FTS $CO_2$ measurements and the extended CMAM, for April, for various scenarios to be discussed below. Since CMAM is a climate model and so does not produce a forecast, comparison with specific dates is inappropriate. However, the CMAM data averaged over the month appropriate for the ACE-FTS measurements should be representative. The ACE-FTS gives a reasonable latitudinal coverage in April and from Fig. 3 we see that the overall structure exhibited by the model for the standard scenario, A, is similar to that of the observations. However, the measurements appear to have more structure with latitude. Also, the initial fall-off of $CO_2$ mixing ratio with height for the ACE measurements is seen to occur at lower altitudes (see also Fig. 4) than for the model results in the control run, scenario A.

One issue which needs to be pointed out, when examining ACE-FTS data, is that specific features in the $CO_2$ and CO datasets may not be accurately compared between the ACE and CMAM results at high latitudes, since the ACE experiment is subject to a sampling bias as data is less frequently observed and so strong shorter lived features may be mis-represented when the data is averaged into monthly bins. However the main analysis discusses the middle and low latitudes where this effect is not as prevalent and the observations are multi-year averages so as to reduce this problem. Though this means specific year gradients will be "smeared" and not well reproduced, but the climatological structure should be reasonably represented. Thus discussion of specific and transient features will be more qualitative whereas the overall climatology can be better assessed. Also in the plots displayed height is shown in most plots as approximate height which as its name implies is not real height, so care must be taken when comparing to other datasets presented as a function of altitude.

Prompted by the disagreement between the model and measurements we have explored the conditions required to produce better agreement between the two. This was undertaken using a series of model sensitivity experiments to explore the processes which might impact the profile in order to reconcile the model and observations. These experiments cover a range of hypothetical extremes of parameter space. The list of scenarios is given in Table 3 and in more detail in the text following. In an attempt to simulate the "knee" occurring at lower altitudes we have increased the photolysis rate for $CO_2$ by a factor of 5; this is scenario B. As the standard scenario A includes eddy diffusion of chemical species associated with parameterized GWD, we introduce a scenario C with $K_{zz}$ (GWD) neglected to explore the impact of mixing by unresolved gravity waves. Scenario D is a simulation that is a combination of B and C, i.e., both an increased photolysis rate for $CO_2$ and the neglect of mixing due to $K_{zz}$ (GWD). In order to explore the contribution of CO recombination to $CO_2$, scenario E assumes a recombination rate for

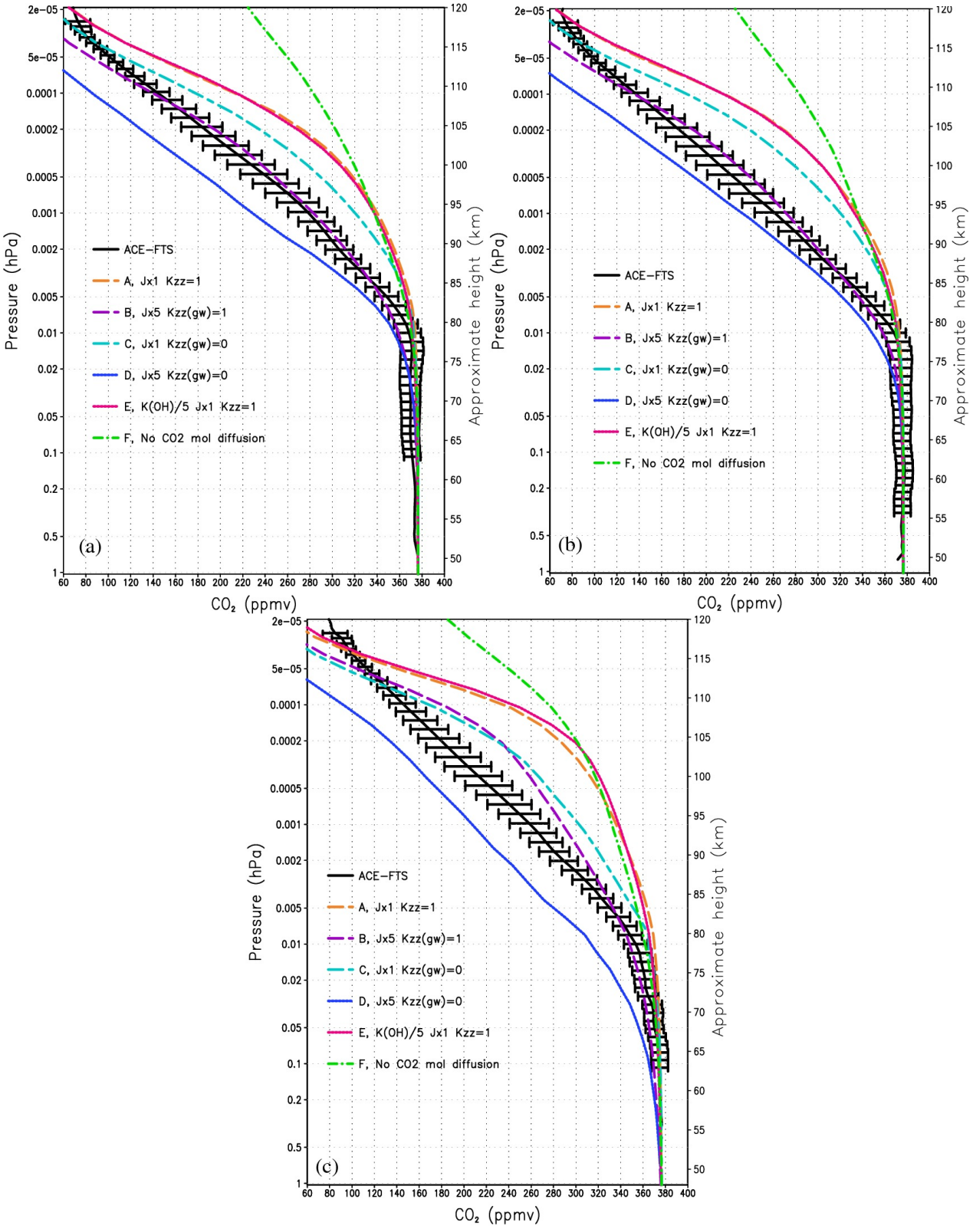


**Fig. 4.** ACE $CO_2$ profiles from Fig. 3, for latitudes **(a)** 30° N, **(b)** 3° N, **(c)** 80° S. Also shown are the CMAM $CO_2$ profiles for the various scenarios in Table 3.

CO and OH to produce $CO_2$ five times slower than the standard rate. For completeness, we have also investigated the impact of molecular diffusion and so for scenario F we have eliminated molecular diffusion for $CO_2$; note that molecular diffusion is retained for all the other species.

The cross-sections for each scenario for the month of April are shown in Fig. 3 and the behaviour is generally what might be expected. Scenario B with the increased $J$ value shows that $CO_2$ is depleted in the MLT region compared to A. There is some difference in the structure in the lower thermosphere where the contours are flatter for B. From scenario C it is clear that eddy diffusion effects from GWD do have an impact, transporting $CO_2$ upwards. The impact of D, i.e. a combination of both B and C, is clearly excessive in terms of reducing the model $CO_2$ field in the MLT. For scenario E, the impact of reduced formation of $CO_2$ from CO is only seen below ∼0.005 hPa, resulting in less $CO_2$. Scenario F has an impact in the mesosphere resulting in a smaller $CO_2$ field. In the lower thermosphere the $CO_2$ field is increased as it is maintained by the resolved wind field and is not constrained by trying to achieve gravity-diffusive equilibrium with a concomitantly smaller scale height.

Figure 4 shows a series of averaged ACE April profiles (together with estimated error bars) for regions where there is ample ACE data, viz., ∼30° N, 3° N, and 80° S. Also shown are the CMAM profiles for the various scenarios listed in Table 3 which highlights more clearly the inability of the model to simulate the height at which the $CO_2$ mixing ratio begins to fall off as shown by the ACE data. At 30° N for April (Fig. 4a) the ACE mixing ratio data indicate a distinct fall-off or "knee" beginning at ∼80 km. All the model results indicate a fall-off in this region but it is not so steep, except for scenarios B and D. Clearly the scenario which gives the best agreement is one where the $J$ value is increased by a factor of five (B) while the worst agreement above 100 km, as might be expected, is F with no molecular diffusion. Only D, with both high $J$ value and no $K_{zz}$ from GWD, lies below the measurements.

Figure 4b shows the same comparison as 30° N for the tropics (3° N) for April. The results are generally the same. Thus the increased $J$ value gives the best agreement with other scenarios generally following those seen in Fig. 4a. For austral polar regions (80° S) the results are shown in Fig. 4c. For this case none of the scenarios provide good agreement. Even scenario B, is a poor fit and scenario D, with modified $J$ and $K_{zz}$ (GWD)=0 is too low. The effect of $K_{zz}$ (GWD) is clearly stronger in the polar regions. The reason for $CO_2$ being diffused upwards to higher altitudes in the polar regions stronger than in the other regions is that the impact of turbulent mixing generated by unresolved gravity wave breaking in the model is most important in the polar regions compared to the tropics and mid-latitude regions (Fig. 5). The role of $K_{zz}$ upon the distributions of $CO_2$ and CO has been studied before and in particular by López-Puertas et al. (2000).

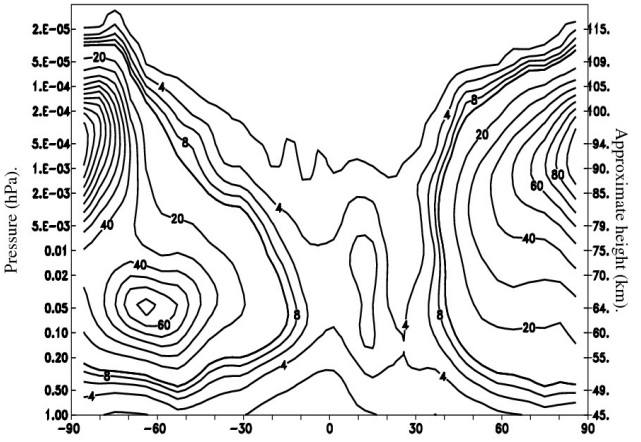


**Fig. 5.** Latitude-pressure plot of $K_{zz}$ (GWD) in $m^2/s$ for April from CMAM. Contour interval of 2 used for values below 10 $m^2/s$ and 10 for values above 10 $m^2/s$.

Figure 6 shows the April CO mixing ratios for ACE and for each of the scenarios for CMAM shown in Table 3. The standard scenario A, suggests that the CMAM simulation of CO provides a generally reasonable representation of CO (outside regions of strong high/mid latitude descent). This is not unexpected as the standard CMAM with a top at 0.001 hPa also simulates well the CO distribution (Jin et al., 2005, 2009). The extended CMAM CO, scenario A, is generally within 30% of the ACE CO, which, considering the rapid vertical variation of CO seems quite reasonable. However, we should bear in mind that the CO production rate calculated from the photolysis of $CO_2$ must be too high above 80 km since the model $CO_2$ field is too high for the control run (A).

For scenario B with increased $J$ value we see that the CO is up to a factor of five too large at most locations and this is with a $CO_2$ distribution which fits the ACE observations; one implication is that the removal process for $CO_2$ cannot simply result in production of CO. For case C with $K_{zz}$ (GWD) turned off the model CO is too low by ∼30% at 0.002 hPa but at 0.2 hPa the model is too high by about 30% as compared to the ACE, so that the gradient has been affected by turning off $K_{zz}$ (GWD). This highlights issues already brought out in López-Puertas et al. (2000) and re-iterated in this paper that the uncertainties in the $K_{zz}$ value needed in the MLT region are important and our understanding of their temporal, vertical and latitudinal variations is lacking in order to correctly identify the role of the turbulence in the motion of species in this region. For case D the model CO is too high by about a factor of 4 which suggests that this scenario is also not reasonable. For case E, where the CO loss has been reduced, above about 0.01 hPa (∼80 km) the CO is only slightly larger than the standard scenario A, reflecting that the CO in this region is largely controlled by dynamics whereas below ∼80 km the larger CO VMRs reflect the slower loss

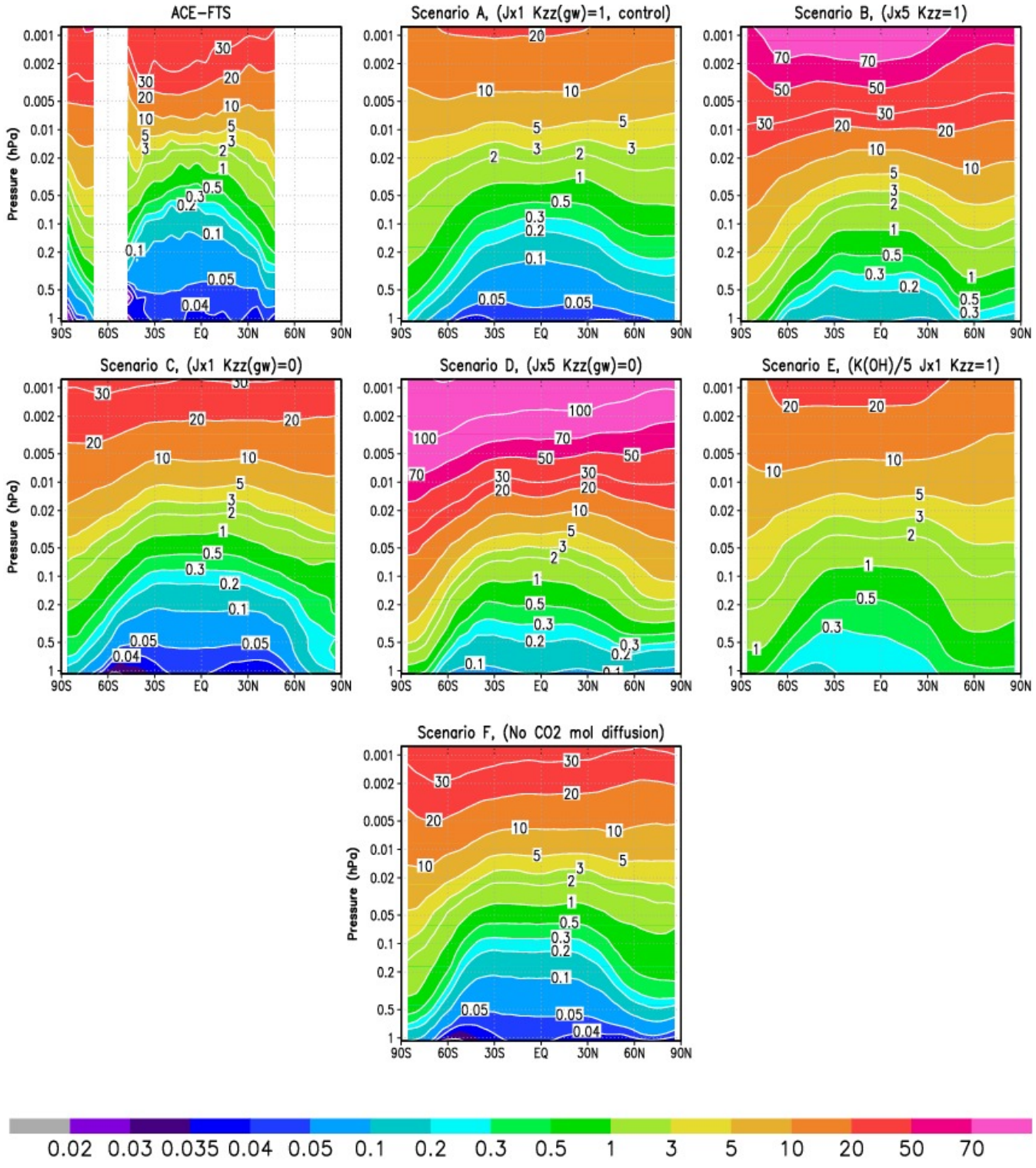


**Fig. 6.** Zonally and monthly averaged latitude-pressure plots of CO volume mixing ratios (ppmv) for April for the different scenarios shown in Table 3 used for the CMAM and the ACE data (details same as Fig. 1).

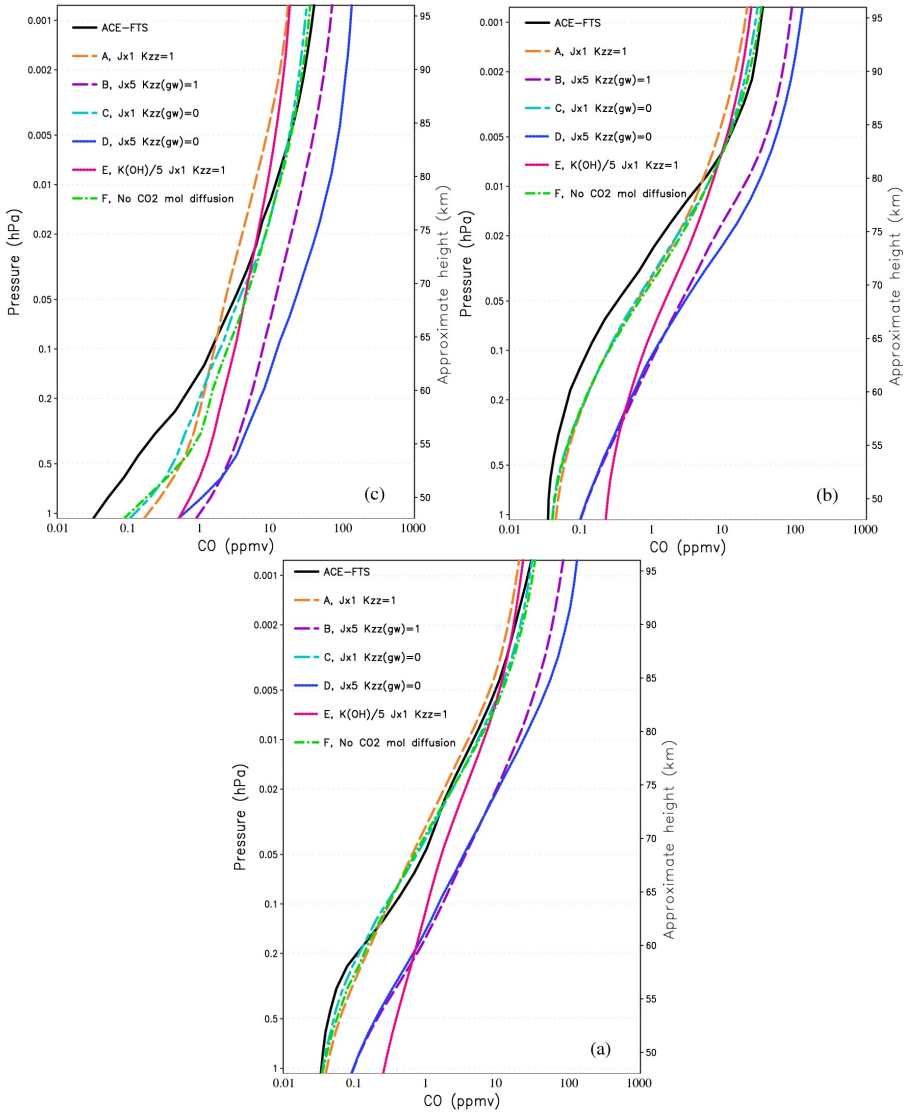


**Fig. 7.** ACE CO profiles from Fig. 6 for latitudes **(a)** 30° N, **(b)** 3° N, **(c)** 80° S. Also shown are the CMAM CO profiles for the various scenarios in Table 3.

process as compared to case A. For case F with molecular diffusion turned off for $CO_2$, the CO increases in the upper part of the domain reflecting higher $CO_2$ concentration in the lower thermosphere.

Similar to Fig. 4, Fig. 7 shows profile data for ACE and CMAM CO at latitudes where there is adequate data, 30° N, 3° N and 80° S. The CMAM data are for the scenarios listed in Table 3. The standard CO profile is in reasonable agreement with the ACE data below 0.01 hPa (∼80 km); above this height it is lower than the observations and is 30% too low by 0.001 hPa (∼95 km) for these latitudes. Case B with increased photolysis is too large by a factor between 4 and 5, varying with height. Given that the model $CO_2$ is in reasonable agreement with the observations for this case, this suggests that the CO source is too large by about a factor of 5. This strongly suggests that increased photolysis cannot solve the problem. This is an important constraint. Scenario C with decreased $K_{zz}$ is in reasonable agreement with the observations (but of course the $CO_2$ does not fit). This CO profile is larger than that for scenario A since the downward diffusion of CO has been decreased with $K_{zz}$ (GWD) = 0. Scenario D is the worst case and the disagreement of scenario B is amplified by the reduction of downward diffusion due to $K_{zz}$. For scenario E the VMRs reflect the slower CO loss rate so that the model mixing ratios are too large below about 0.005 hPa (∼85 km). The effect of the zeroing molecular diffusion for $CO_2$ (scenario F) increases CO due to larger VMRs of $CO_2$ in the lower thermosphere. For the tropics the comparison is similar. Scenarios B and D produce CO mixing ratios that are much too large compared to the ACE observations. The

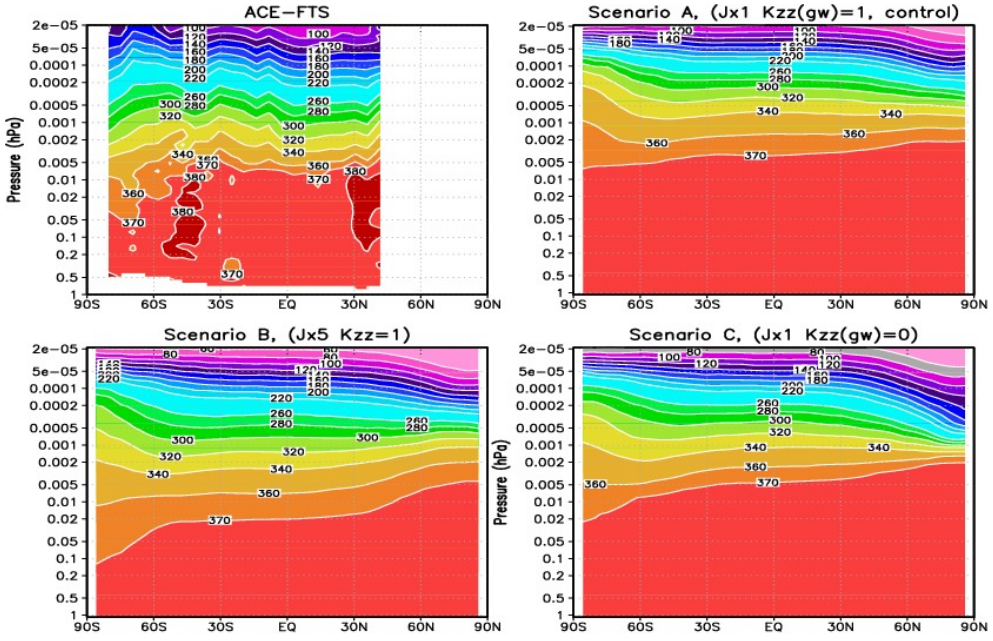


**Fig. 8.** Zonally and monthly averaged latitude-pressure plots of $CO_2$ volume mixing ratios (ppmv) for August for the different scenarios shown in Table 3 used for the CMAM and the ACE data (details same as Fig. 1).

other scenarios are generally too low above about 80 km. For the austral polar region, similar behaviour is exhibited as for the other latitudes. Although we note that none of the model results give agreement below 0.1 hPa and the standard run is too small by a factor of 2 at ∼0.001 hPa.

The above has focused on vernal equinox. We now investigate the late northern summer, August, to ensure that the same characteristics prevail for all seasons. August is a month where the ACE data has adequate coverage from the northern sub-tropics to the austral polar regions (see Fig. 1). Figure 8 shows the ACE $CO_2$ data for August and the CMAM data for the scenarios A, B and C (Table 3). A comparison of the ACE data with the standard scenario A, shows that the behaviour is similar in August as for April in that the measured $CO_2$ begins to fall off at lower altitudes than does the model. We note that the slopes of the ACE contours in the polar region are affected by sampling as for April as can also be seen in Jin et al. (2009). However, there are qualitative differences between April and August for the other scenarios. For example, scenario B with an increased $J$ value is now excessive, in that the CMAM $CO_2$ falls off too rapidly in this case. Scenario C with $K_{zz}$ (GWD) turned off produces results where $CO_2$ is too high. We have also looked at the plots (not shown) for specific latitudes as for April and the above behaviour is confirmed.

Figure 9 presents the plots for August for CO for ACE data and the Table 3 scenarios of CMAM. The control scenario A, gives quite good agreement below about 0.05 hPa but is about a factor of 2 low at 0.001 hPa and the latitudinal behaviour is quite similar. For scenario B, the CO is generally too high by up to a factor of five which again suggests that an increased $J$ value is not the solution for the poor fit for the control. Scenario C with a decreased $K_{zz}$ leads to somewhat better agreement with the observation in the upper mesosphere than scenario A, as the CO is not diffused down as rapidly. In the lower regions, where the CO abundance is mainly controlled by chemistry, the CO distributions for cases A and C are very similar.

## 5 Discussion

As far as we can discern this is the first published 3-dimensional (3-D) study of $CO_2$ in the MLT region using a GCM with a vertical domain that extends from the surface to the thermosphere. As noted above, Kaufmann et al. (2002) presented a 3-D study of $CO_2$ using the TIME-GCM. This is a 3-D time dependent GCM extending from 30 to 500 km, and for their calculations they used a $5^\circ \times 5^\circ$ horizontal resolution with two grid points per scale height in the vertical and a 4 min time step (see for example Roble, 1995) and references therein for a more detailed description of the TIME-GCM). Kaufmann et al. (2002) found problems, similar to what we have elucidated above, with the differences of the vertical distributions of $CO_2$ mixing ratio between measurements and model. Mertens et al. (2009a) find similar discrepancies between the SABER V1.06 $CO_2$ profiles and the TIME-GCM. Chabrillat et al. (2002) have used a 2-D model to investigate the impact of molecular diffusion on the $CO_2$ distribution in the MLT region. They obtained reasonable

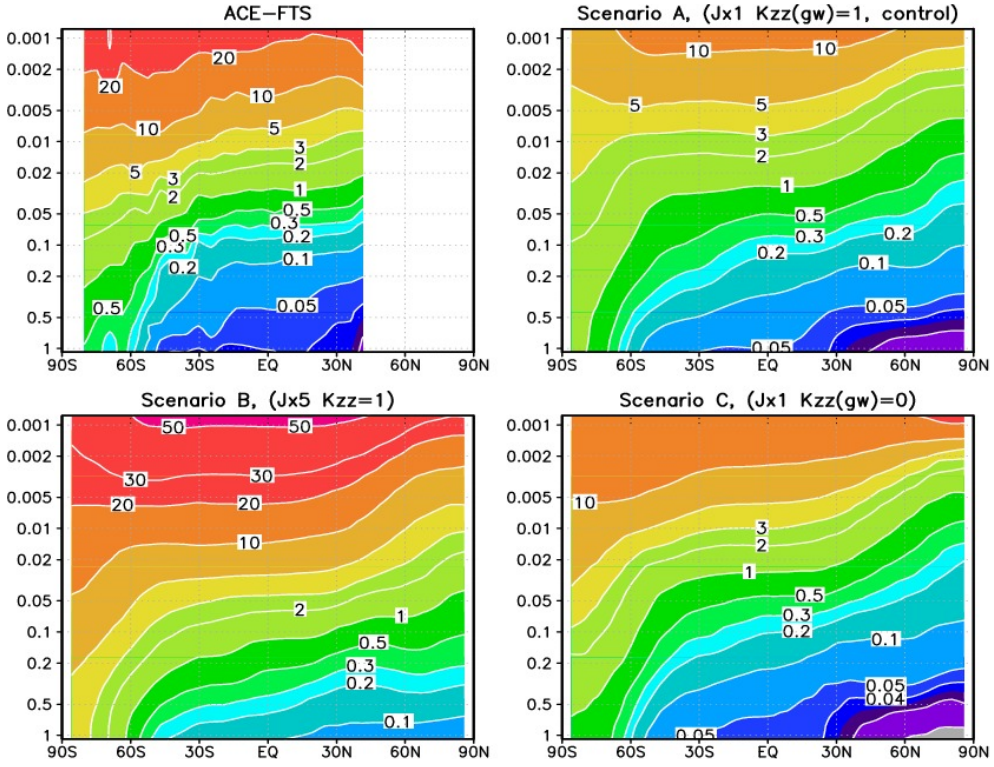


**Fig. 9.** Zonally and monthly averaged latitude-pressure plots of CO volume mixing ratios (ppmv) for August for the different scenarios shown in Table 3 used for the CMAM and the ACE data (details same as Fig. 1).

agreement with the rocket measurements but did not explicitly compare with the CRISTA-1 measurements which have a "knee" much lower.

The figures presented above explore a series of sensitivity tests to examine the major processes which affect the $CO_2$ vertical profile. It is clear that the model can only reproduce a fall-off similar to that seen in ACE when the photolysis is increased significantly, far beyond any reasonable uncertainty in the known parameters determining the photolysis in this region. Other factors such as the magnitude of turbulence generated by breaking of the unresolved gravity waves, uncertainties in the $CO_2$ reformation rates and the action of molecular diffusion at these altitudes seem unable to produce the correct change in distribution of the $CO_2$. We note that the application of $K_{zz}$ (GWD) is not a standard feature of middle atmosphere models. To our best knowledge, there are only two GWD parameterizations (Hines, 1997a, b; Lindzen, 1981) which provide eddy diffusion coefficients. That is why we have investigated the impact of $K_{zz}$ (GWD) removal. In addition, the resolved circulation in the middle atmosphere is quite sensitive to the tuning of GWD parameterizations and this can also affect the species distribution as much as $K_{zz}$ (GWD). Given the uncertainty in our knowledge of the effects of diffusion generated by gravity wave breaking, a major contributor to the $K_{zz}$ in this region, some concern over the role and strength of gravity wave induced motion is warranted. However, even if we neglect all diffusive transport associated with unresolved gravity wave breaking, the $CO_2$ vertical profile does not begin to fall off in the model as low as the ACE observations indicate. Nevertheless we note that for other species in the MLT region, such as $H_2O$, $N_2O$, $CH_4$, as well as $CO_2$, for which their distributions are determined by vertical transport balanced by chemical loss, that knowledge of $K_{zz}$ is important in the determination of their distributions (see also Jin et al., 2009).

Although the photolysis rate of $CO_2$ appears reasonably well characterized, except, as noted above, at longer wavelengths, we have estimated what increase might be required to produce agreement (without consideration of CO): this is scenario B. This scenario appears to be the only simulated process capable of reconciling the mesospheric $CO_2$ fall-off in the model and observations amongst the scenarios considered. Although, based on the current knowledge, we could not find any physical reasons for the $CO_2$ photolysis to be a few times larger than that used in scenario A, results from scenario B clearly indicate that some additional $CO_2$ loss processes are required in the mesosphere in order to reconcile the model and observations.

In the height region of interest, between approximately 70 and 100 km, the $CO_2$ molecule is photolyzed mainly in the Lyman-$\alpha$ line. In this case the value of the photolysis rate depends on $CO_2$ and $O_2$ cross sections in the

vicinity of Lyman-$\alpha$ and on the level of solar activity. The solar flux in the Lyman-$\alpha$ line varies by about 30% from solar maximum to solar minimum. However, for the period of the ACE observations (2004–2007), the solar irradiance at Lyman-$\alpha$ line reported on the SOLARIS website (http://www.geo.fu-berlin.de/en/met/ag/strat/forschung/SOLARIS/Input_data/index.html) does not differ by more than 10% from that used in our calculation, with our value being generally larger.

The $CO_2$ cross section at Lyman-$\alpha$ for about 300 K reported by different authors varies between $(6.5–8.2)\times10^{-20}$ cm$^2$ (e.g. see Yoshino et al., 1996). There is also a weak temperature dependence: the cross section slowly increases with temperature at 0.1%/K (Lewis and Carver, 1983). Some uncertainties exist in what temperature the cross section should be taken at. The kinetic temperature in the upper mesosphere is generally lower than 200 K. However, there is some justification for higher temperatures being used. This is because the vibrational levels of $CO_2$ are non-thermally excited in the mesosphere so that daytime vibrational temperatures are higher than the kinetic temperature (e.g., López-Puertas and Taylor, 2001). We have estimated potential impact of non-LTE on the $CO_2$ cross-section by considering the upper limit of the effect and found out that non-LTE effects cannot likely lead to a considerable increase in the $CO_2$ photolysis rate. Daytime $CO_2$ vibrational temperatures do not exceed 250 K and 350 K for the lower and higher vibrational levels, respectively (e.g., López-Puertas and Taylor, 2001). Given the temperature dependence of the $CO_2$ cross section to be 0.1%/K, the latter means that non-thermal excitation of the $CO_2$ vibrational levels cannot lead to a cross section increase of more than $\sim$5% from the value measured at 300 K.

Chabrillat and Kockarts (1997) have noted that because of the structure in the $O_2$ absorption cross section in the vicinity of Lyman-$\alpha$ that $J$ values for $H_2O$ and $CH_4$ are affected to varying degrees. Thus we have evaluated the impact on $J(CO_2)$ and find that its uncertainty is less than 15% in the height region of interest so that its contribution to the uncertainty is much less than is required by our comparisons. Also $J(CO_2)$ is rather uncertain at longer wavelengths both versus wavelength and temperature (Parkinson et al., 2003; Shemansky, 1972; Karaiskou et al., 2004). However this long wavelength uncertainty should only affect $J(CO_2)$ for altitudes below about 65 km (see, for example, Brasseur and Solomon, 2005) and not impact our calculations. For the $CO_2$ cross section in the Lyman-$\alpha$ region we use a value of $7.7\times10^{-20}$ cm$^2$ which suggests that even with all the uncertainties taken into account, we rather overestimate the $CO_2$ photolysis rate in the upper mesosphere than underestimate it.

CO provides an important additional constraint on the problem of the carbon distribution in the MLT region. CO is created from the $CO_2$ photolysis and is advected and diffused from above. In the model control simulation, scenario A, CMAM CO is up to a factor of two too low above 0.01 hPa (80 km). But even though the source, $CO_2$, is too high and the $J$ value should be appropriate, the CO is low. As noted above there is no clear evidence to suggest a serious error in the photolysis rate of $CO_2$ at these altitudes. A number of the sensitivity experiments do create higher CO levels at the pressure range required to mimic the ACE observations, viz., scenarios B (enhanced photolysis of $CO_2$), C (reduced $K_{zz}$), and F (molecular diffusion=0) as can be seen from Figs. 6, 7 and 9. A change in $K_{zz}$ could be envisaged to get CO closer to the ACE observations but a neglect of molecular diffusion (namely no gravitational separation of $CO_2$) is physically unreasonable. And, as we have seen in Figs. 6, 7 and 9, the $J$ value enhancement (scenario B) results indicate that the concomitant increase in CO is too large compared to the ACE observations. For this scenario the agreement between measured and modeled CO has worsened above 65 km with the source of CO having increased dramatically and unrealistically.

The impact of scenario C ($K_{zz}$ (GWD)=0) is to effect a fall-off in $CO_2$ at lower altitudes as the upward transport of $CO_2$ down the mixing ratio gradient has been decreased. We note that the agreement between model and measurements is improved somewhat but that the model $CO_2$ still remains too high. López-Puertas et al. (2000) show in their Fig. 7 that a reduced $K_{zz}$ can, using a 1-D global model, make a big difference in the $CO_2$/CO profiles lowering the "knee" and altering the $CO_2$ profile significantly above 100 km. However the lower $K_{zz}$ results were not directly compared to observations or applied to a 3-D GCM in their paper. Our results do not show as large a sensitivity to turbulent parameterized diffusion when undertaken within a 3-D GCM suggesting that resolved waves and transport may be part of the extra transport seen in CMAM and represented as $K_{zz}$ in the 1-D tests from Lopez-Puertas at al. (2000). In this context it might be of importance to consider how well the extended CMAM simulates temperatures. Figure 10 presents zonally and temporally averaged latitude-pressure temperature for ACE and the CMAM control run for April and August. Bearing in mind that there are sampling limitations for ACE, the agreement between temperatures is rather good. This suggests that the CMAM is capable of adequately modeling the large scale circulation and, hence, transport due to the resolved dynamics.

Although the experiments with reduced $K_{zz}$ (GWD) are not the full solution to the current discrepancy between the ACE observations and model, they are, however, revealing. It is clear that the Hines GWD induced $K_{zz}$ may play an important role in the vertical transport of species in the mesosphere for some species such as CO, NO, $CH_4$, $N_2O$, $H_2O$ as well as $CO_2$ but its vertical and latitudinal structure has not been thoroughly explored. It would be interesting to investigate the impact of $K_{zz}$ fields derived from other GWD schemes. As noted above each GWD scheme will induce not just a different dynamical and temperature structure but also

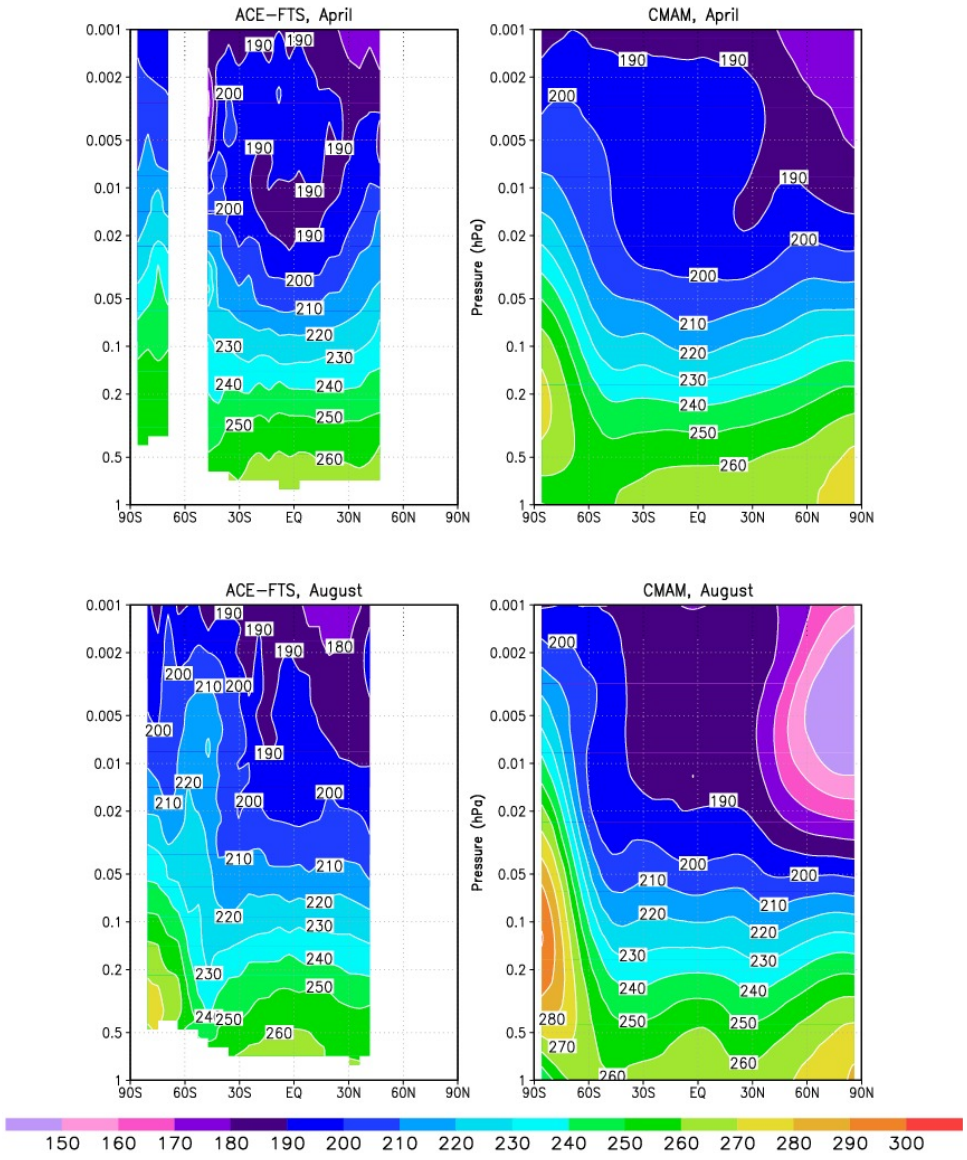


**Fig. 10.** Zonally and monthly averaged latitude-pressure plots of temperature (K) for the ACE data and for the control run (scenario A) for the CMAM for April (top panels) and August (bottom panels).

a different species structure and by choosing suitable species it may be possible to further constrain GWD parameterizations.

As is clear from above results, the most reasonable scenario for agreement between the ACE $CO_2$ observations and CMAM simulations is with an increased $J$ value (perhaps with a different enhancement factor between April and August). However, the concomitant increased source of CO is not present in the observations. This is then suggestive that carbon may be sequestered elsewhere in the atmospheric system. At this point our only suggestion is perhaps $CO_2$ may react with meteoritic dust in the mesosphere. A possible mechanism for the carbon removal on the mesospheric dust is described in Plane (2004). Estimating reaction times at ∼80 km using typical meteoritic surface areas (e.g., Megner et al., 2008) we obtain $9/\gamma$ h where $\gamma$ is the efficiency for non-reversible reaction on the dust, this should be compared with $1/J(CO_2)$ for Lyman-$\alpha$ at 80 km which is ∼13 days for a diurnal average at mid-latitudes. Thus $\gamma$=0.1 would yield a loss process ∼3–5 times faster than photolysis. This could yield a faster $CO_2$ removal rate while not producing CO. If this in fact proves to be the case then one might expect other similar reactions to be occurring on meteoritic dust. An interesting feature of such a phenomenon is that it will be spatially and temporally variable so that its effects will vary from season to season with varying dust amounts which might account for the variation required in the "enhanced" $J(CO_2)$ to account for the observations in April and August.

## 6 Summary

We present the first global set of observations of ground state $CO_2$ for the mesosphere and lower thermosphere. We also present the measurements of CO obtained concurrently. They were obtained by the ACE-FTS instrument on SCISAT-I, a small Canadian satellite, using solar occultation. There are certain limitations on seasonal and zonal averages due to the particular orbit which emphasizes investigations of polar regions and also due to the particular sampling properties of solar occultation. The $CO_2$ mixing ratio distribution from ACE lies between the CRISTA-1 values (Kaufmann et al., 2002) and the rocket values (compilation by Fomichev et al., 1998) and is similar to the SABER V1.06 measurements (Mertens et al., 2009b).

We have compared the ACE measurements to calculations of the $CO_2$ and CO distributions using the extended Canadian Middle Atmosphere Model (CMAM) which has a lid at about 220 km. Applying standard chemistry we find that we cannot get agreement between the ACE observations and CMAM simulations in the mesosphere and, in particular, the model cannot reproduce adequately the height of the "knee", i.e. the height at which $CO_2$ begins to fall off while adequately reproducing the CO observations. We have investigated the variation of several parameters of interest in order to explore parameter space for this problem. Our conclusions are that there must be a loss process for $CO_2$ that will sequester the carbon in some form other than CO; we have speculated on the role of meteoritic dust. We also highlight the important role for $K_{zz}$, viz. eddy diffusion of species associated with GWD.

*Acknowledgements.* We would like to thank the two referees, Manuel López-Puertas and Martin Kaufmann, who provided useful comments. The authors would like to acknowledge support by the Canadian Space Agency (CSA), the Natural Sciences and Engineering Research Council (NSERC) of Canada, the Canadian Foundation for Climate and Atmospheric Science (CFCAS), the Canadian Foundation for Innovation, the Ontario Innovation Trust and the UK Natural Environment Research Council.

Edited by: W. Ward

## References

Beagley, S. R., McLandress, C., Fomichev, V. I., and Ward, W. E.: The extended Canadian Middle Atmosphere Model, Geophys. Res. Lett., 27(16), 2529–2532, 2000.

Beagley, S. R., McConnell, J. C., Fomichev, V. I., Semeniuk, K., Jonsson, A. I., Garcia Munoz, A, McLandress, C., and Shepherd, T. G.: Extended CMAM: Impacts of thermospheric neutral and ion chemistry on the middle atmosphere, AGU, fall, 2007.

Bernath, P. F., McElroy, C. T., Abrahams, M. C., Boone, C. D., Butler, M., Camy-Peyret, C., Carleer, M., Clerbaux, C., Coheur, P. F., Colin, R., DeCola, P., DeMazire, M., Drummond, J. R., Dufour, D., Evans, W. F. J., Fast, H., Fussen, D., Gilbert, K., Jennings, D. E., Llewellyn, E. J., Lowe, R. P., Mahieu, E., McConnell, J. C., McHugh, M., McLeod, S. D., Michaud, R., Midwinter, C., Nassar, R., Nichitiu, F., Nowlan, C., Rinsland, C. P., Rochon, Y. J., Rowlands, N., Semeniuk, K., Simon, P., Skelton, R., Sloan, J. J., Soucy, M.-A., Strong, K., Tremblay, P., Turnbull, D., Walker, K. A., Walkty, I., Wardle, D. A., Wehrle, V., Zander, R., and Zou, J.: Atmospheric Chemistry Experiment (ACE): Mission overview, Geophys. Res. Lett., 32, L15S01, doi:10.1029/2005GL022386, 2005.

Boone, C. D., Nassar, R., Walker, K. A., Rochon, Y., McLeod, S. D., Rinsland, C. P., and Bernath, P. F.: Retrievals for the atmospheric chemistry experiment Fourier-transform spectrometer, Appl. Opt., 44(33), 7218–7231, 2005.

Brasseur, G. P. and Solomon, S.: Aeronomy of the Middle Atmosphere: Chemistry and Physics of the Stratosphere and Mesosphere, third revised and enlarged ed., Springer, Nordrecht, The Netherlands, 646 pp., 2005.

Chabrillat, S. and Kockarts, G.: Simple parameterization of the absorption of the solar Lyman-alpha line, Geophys. Res. Lett., 24, 2659–2662, 1997.

Chabrillat, S., Kockarts, G., Fonteyn, D., and Brasseur, G.: Impact of molecular diffusion on the $CO_2$ distribution and the temperature in the mesosphere, Geophys. Res. Lett., 29, 1729, doi:10.1029/2002GL015309, 2002.

Davis, S. P., Abrams, M. C., and Brault, J. W.: Fourier Transform Spectroscopy, Academic Press, London, 262 pp., 2001.

de Grandpré, J., Beagley, S. R., Fomichev, V. I., Griffioen, E., McConnell, J. C., Medvedev, A. S., and Shepherd, T. G.: Ozone climatology using interactive chemistry: Results from the Canadian Middle Atmosphere Model, J. Geophys. Res., 105(D21), 26475–26492, doi:10.1029/2000JD900427, 2000.

Edwards, D. P., Kumer, J. B., López-Puertas, M., Mlynczak, M. G., Gopalan, A., Gille, J. C., and Roche, A.: Non-local thermodynamic equilibrium limb radiance near 10 µm as measured by UARS CLAES, J. Geophys. Res., 101, 26577–26588, 1996.

Edwards, D. P., López-Puertas, M., and Gamache, R. R.: The non-LTE correction to the vibrational component of the internal partition sum for atmospheric calculations, J. Quant. Spectrosc. Ra., 59, 423–436, 1998.

European Organization for the safety of Air Navigation, Brussels, Belgium, the Institute of Geodesy and Navigation, University FAF, Munich, Germany, WGS 84 Implementation Manual Version 2.4, 1998.

Fomichev, V. I., Blanchet, J.-P., and Turner, D. S.: Matrix parameterization of the 15 µm $CO_2$ band cooling in the middle and upper atmosphere for variable $CO_2$ concentration, J. Geophys. Res., 103, 11505–11528, 1998.

Fomichev, V. I., Ward, W. E., Beagley, S. R., McLandress, C., McConnell, J. C., McFarlane, N. A., and Shepherd, T. G.: Extended Canadian Middle Atmosphere Model: Zonal-mean climatology and physical parameterizations, J. Geophys. Res., 107(D10), 4087, doi:10.1029/2001JD000479, 2002.

Girard, A., Besson, J., Brard, D., Laurent, J., Lemaitre, M. P., Lippens, C., Muller, C., Vercheval, J., and, Ackerman, M.: Global results of grille spectrometer experiment on board Spacelab 1, Planet. Space Sci., 36, 291–300, 1988.

Hines, C. O.: Doppler-spread parameterization of gravity-wave momentum deposition in the middle atmosphere. Part 1: Basic formulation, J. Atmos. Sol.-Terr. Phys., 59, 371–386, 1997a.

Hines, C. O.: Doppler-spread parameterization of gravity-wave momentum deposition in the middle atmosphere. Part 2: Broad and quasi-monochromatic spectra, and implementation, J. Atmos. Sol.-Terr. Phys., 59, 387–400, 1997b.

Jin, J. J., Semeniuk, K., Jonsson, A. I., Beagley, S. R., McConnell, J. C., Boone, C. D., Walker, K. A., Bernath, P. F., Rinsland, C. P., Dupuy, E., Ricaud, P., De la Noe, J., Urban, J., and Murtagh, D.: A comparison of co-located ACE-FTS and SMR stratospheric-mesospheric CO measurements during 2004 and comparison with a GCM, Geophys. Res. Letts, 32, L15S03, doi:10.1029/2005GL022433, 2005.

Jin, J. J., Semeniuk, K., Beagley, S. R., Fomichev, V. I., Jonsson, A. I., McConnell, J. C., Urban, J., Murtagh, D., Manney, G. L., Boone, C. D., Bernath, P. F., Walker, K. A., Barret, B., Ricaud, P., and Dupuy, E.: Comparison of CMAM simulations of carbon monoxide (CO), nitrous oxide ($N_2O$), and methane ($CH_4$) with observations from Odin/SMR, ACE-FTS, and Aura/MLS, Atmos. Chem. Phys., 9, 3233–3252, 2009, http://www.atmos-chem-phys.net/9/3233/2009/.

Karaiskou, A., Vallance, C., Papadakis, V., Vardavas, I. M., and Rakitzis, T. P.: Absolute absorption cross-section measurements of $CO_2$ in the ultraviolet from 200 to 206 nm at 295 and 373 K , Chem. Phys. Lett., 400, 30–34, 2004.

Kaufmann, M., Gusev, O. A., Grossmann K. U., Roble, R. G., Hagan, M. E., Hartsough, C., and Kutepov, A. A.: The vertical and horizontal distribution of $CO_2$ densities in the upper mesosphere and lower thermosphere as measured by CRISTA, J. Geophys. Res., 107(D23), 8182, doi:10.1029/2001JD000704, 2002.

Kaye, J. A. and Miller, T. L.: The ATLAS series of shuttle missions, Geophys. Res. Lett., 23, 2285–2288, 1996.

Kumer, J. B., Stair Jr., A. T., Wheeler, N., Baker, K. D., and Baker, D. J.: Evidence for an $OH^{\neq} \xrightarrow{v v} N_2^{\neq} \xrightarrow{v v} CO_2(\nu_3) \longrightarrow CO_2 + h\nu$ (4.3 µm) mechanism for 4.3-µm airglow, J. Geophys. Res., 83, 4743–4747, 1978.

Lewis, B. R. and Carver, J. H.: Temperature dependence of the carbon dioxide photoabsorption cross section between 1200 and 1970 Å, J. Quant. Spectrosc. Ra., 30, 297–309, 1983.

Lindzen R. S.: Turbulence and stress owing to gravity wave and tidal breakdown, J. Geophys. Res., 86, 9704–9714, 1981.

López-Puertas, M. and Taylor, F. W.: Carbon dioxide 4.3 µm emission in the Earth's atmosphere: A comparison between NIMBUS 7 SAMS measurements and non-local thermodynamic equilibrium radiative transfer calculations, J. Geophys. Res., 94, 13045–13068, 1989.

López-Puertas, M., Zaragoza, G., López-Valverde, M. A., and Taylor, F. W.: Non local thermodynamic equilibrium (LTE) atmospheric limb emission at 4.6 µm 2, An analysis of the daytime wide-band radiances as measured by UARS improved stratospheric and mesospheric sounder, J. Geophys. Res., 103, 8515–8530, 1998.

López-Puertas, M., Lopez-Valverde, M. A., Garcia, R. R., and Roble, R. G.: A review of $CO_2$ and CO abundances in the middle atmosphere, in: Atmospheric Science Across the Stratopause, edited by: Siskind, D. E., Eckermann, S. D., Summers, M. E., AGU, Washington D. C., Geoph. Monog. Series, 123, 83–100, 2000.

López-Puertas, M. and Taylor, F. W.: Non-LTE Radiative Transfer in the Atmosphere. World Scientific, Singapore/New Jersey/London/Hong Kong, 487 pp., 2001.

López-Puertas, M., García-Comas, M., Funke, B., Picard, R. H., Winick, R., Wintersteiner, P. P., Mlynczak, M. G., Mertens, C. J., Russell III, J. M., and Gordley, L. L.: Evidence for an OH($\upsilon$) excitation mechanism of $CO_2$ 4.3 µm nighttime emission from SABER/TIMED measurements, J. Geophys. Res., 109, D09307, doi:10.1029/2003JD004383, 2004.

McLandress, C., Ward, W. E., Fomichev, V. I., Semeniuk, K., Beagley, S. R., McFarlane, N. A., and Shepherd, T. G.: Large-scale dynamics of the mesosphere and lower thermosphere: An analysis using the extended Canadian Middle Atmosphere Model, J. Geophys. Res., 111, D17111, doi:10.1029/2005JD006776, 2006.

Megner, L., Siskind, D. E., Rapp, M., and Gumbel, J.: Global and temporal distribution of meteoric smoke: A two-dimensional simulation study, J. Geophys. Res., 113, D03202, doi:10.1029/2007JD009054, 2008.

Mertens, C. J., Winick, J. R., Picard, R. H., Evans, D. S., López-Puertas, M., Wintersteiner, P. P., Xu, X., Mlynczak, M. G., and Russell III, J. M.: Influence of solar-geomagnetic disturbances on SABER measurements of 4.3 µm emission and the retrieval of kinetic temperature and carbon dioxide, Adv. Space Res., 43, 1325–1336, 2009a.

Mertens, C. J., Russell III, J. M., Mlynczak, M. Y., She, C.-Y., Schmidlin, F. J., Goldberg, R. A., López-Puertas, M., Wintersteiner, P. P., Picard, R. H., Winick, J. R., and Xu, X.: Kinetic temperature and carbon dioxide from broadband infrared limb emission measurements taken from the TIMED/SABER instrument, Adv. Space Res., 43, 15–27, 2009b.

Nebel, H., Wintersteiner, P. P., Picard, R. H., Winick, J. R., and Sharma, R. D.: $CO_2$ non-local thermodynamic equilibrium radiative excitation and infrared day-glow at 4.3 µm: Application to spectral infrared rocket experiment data, J. Geophys. Res., 99, 10409–10419, 1994.

Offermann, D. and Grossmann, K. U.: Thermospheric density and compositions as determined by a mass spectrometer with cryo ion source, J. Geophys. Res., 78, 8296–8304, 1973.

Offermann, D., Friedrich, V., Ross, P., and Von Zahn, U.: Neutral gas composition measurements between 80 and 120 km, Planet. Space Sci., 29, 747–764, 1981.

Ogibalov V. P. and Fomichev, V. I.: Parameterization of solar heating by the near IR $CO_2$ bands in the mesosphere, Adv. Space Res., 32, 759–764, 2003.

Parkinson, W. H., Rufus, J., and Yoshino, K.: Absolute absorption cross section measurements of $CO_2$ in the wavelength region 163–200 nm and the temperature dependence, Chem. Phys., 290, 251–256, 2003.

Philbrick, C. R., Faucher, G. A., and Trzcinski, E.: Rocket measurements of mesospheric and lower thermospheric composition, Space Research, 13, 255–260, Akademie, Berlin, 1973.

Picone, J. M., Hedin, A. E., Drob, D. P., and Aikin, A. C.: NRLMSISE-00 empirical model of the atmosphere: Statistical comparisons and scientific issues, J. Geophys. Res., 107(A12), 1468, doi:10.1029/2002JA009430, 2002.

Plane, J. M. C.: A time-resolved model of the mesospheric Na layer: constraints on the meteor input function, Atmos. Chem. Phys., 4, 627–638, 2004, http://www.atmos-chem-phys.net/4/627/2004/.

Remsberg, E. E., Marshall, B. T., Garcia-Comas, M., Krueger, D., Lingenfelser, G. S., Martin-Torres, J., Mlynczak, M. G., Russell III, J. M., Smith, A. K., Zhao, Y., Brown, C., Gordley, L. L., López-Gonzalez, M. J., López-Puertas, M., She, C.-Y., Tay-

lor, M. J., and Thompson, R. E.: Assessment of the quality of the Version 1.07 temperature-versus-pressure profiles of the middle atmosphere from TIMED/SABER, J. Geophys. Res., 113, D17101, doi:10.1029/2008JD010013, 2008.

Rinsland, C., Gunson, M. R., Zander, R., and López-Puertas, M.: Middle and upper atmosphere pressure-temperature profiles and the abundances of $CO_2$ and CO in the upper atmosphere from ATMOS/Spacelab 3 observations, J. Geophys. Res., 97, 20479–20495, 1992.

Roble, R. G.: Energetics of the mesosphere and thermosphere, in: The Upper Mesosphere and Lower Thermosphere: A Review of Experiment and Theory, edited by: Johnson R. M. and Killeen, T. L., AGU, Washington D. C., Geoph. Monog. Series, 87, 1–21, 1995.

Rothman, L. S., Jacquemart, D., Barbe, A., Benner, C. C., Birk, M., Brown, L. R., Carleer, M. R., Chackerian Jr., C., Chance, K., Coudert, K. H., Dana, V., Devi, V. M., Flaud, J.-M., Gamache, R. R., Goldman, A., Hartmann, J.-M., Jucks, K. W., Maki, A. G., Mandin, J.-Y., Massie, S. T., Orphal, J., Perrin, A., Rinsland, C. P., Smith, M. A. H., Tennyson, J, Tolchenov, R. N., Toth, R. A., Vander Auwera, J., Varanasi, P., and Wagner, G.: The HITRAN 2004 molecular spectroscopic database, J. Quant. Spectrosc. Ra., 96, 139–204, 2005.

Russell III, J. M., Gordley, L. L., Park, J. H., Drason, S. R., Hesketh, D. H., Cicerone, R. J., Tuck, A. F., Frederick, J. E., Harries, J. E., and Crutzen, P. J.: The Halogen Occultation Experiment, J. Geophys. Res., 98, 10777–10797, 1993.

Schulz, C., Koch, J. D., Davidson, D. F., Jeffries, J. B., and Hanson, R. K.: Ultraviolet absorption spectra of shock-heated carbon dioxide and water between 900 and 3050 K, Chem. Phys. Lett., 355, 82–88, 2002.

Sica, R. J., Izawa, M. R. M., Walker, K. A., Boone, C., Petelina, S. V., Argall, P. S., Bernath, P., Burns, G. B., Catoire, V., Collins, R. L., Daffer, W. H., De Clercq, C., Fan, Z. Y., Firanski, B. J., French, W. J. R., Gerard, P., Gerding, M., Granville, J., Innis, J. L., Keckhut, P., Kerzenmacher, T., Klekociuk, A. R., Kyrö, E., Lambert, J. C., Llewellyn, E. J., Manney, G. L., McDermid, I. S., Mizutani, K., Murayama, Y., Piccolo, C., Raspollini, P., Ridolfi, M., Robert, C., Steinbrecht, W., Strawbridge, K. B., Strong, K., Stbi, R., and Thurairajah, B.: Validation of the Atmospheric Chemistry Experiment (ACE) version 2.2 temperature using ground-based and space-borne measurements, Atmos. Chem. Phys., 8, 35–62, 2008, http://www.atmos-chem-phys.net/8/35/2008/.

Shemansky, D. E.: $CO_2$ Extinction Coefficient 1700–3000 Å, J. Chem. Phys., 56, 1582–1587, 1972.

Trinks, H. and Fricke, K. H.: Carbon dioxide concentrations in the lower thermosphere, J. Geophys. Res., 83, 3883–3886, 1978.

Yoshino, K., Esmond, J. R., Sun, Y., Parkinson, W. H., Ito, K., and Matsui, T.: Absorption cross section measurements of carbon dioxide in the wavelength region 118.7–175.5 nm and the temperature dependence, J. Quant. Spectrosc. Ra., 55, 53–60, 1991.

Zaragoza, G., López-Puertas, M., López-Valverde, M. A., and Taylor, F. W.: Global distribution of $CO_2$ in the upper mesosphere as derived from UARS/ISAMS measurements, J. Geophys. Res., 105, 19829–19839, 2000.